APTAMER-BASED BIOSENSORS FOR REAL-TIME DETECTION OF *LISTERIA MONOCYTOGENES* USING pH-RESPONSIVE POLYMER NANOBRUSHES AND METALLIC NANOPARTICLE PLATFORMS

A Thesis

by

SULEIMAN ABDULLAH S. ALTHAWAB

Submitted to the Office of Graduate and Professional Studies of
Texas A&M University
in partial fulfillment of the requirements for the degree of

MASTER OF SCIENCE

Chair of Committee,	Carmen Gomes
Committee Members,	Elena Castell-Perez
	Matthew Taylor
Head of Department,	Boon Chew

August 2017

Major Subject: Food Science & Technology

ABSTRACT

Listeria monocytogenes is the third most frequent cause of death from foodborne illnesses in the United States. Conventional methods for detecting *L. monocytogenes* are time-consuming and require highly trained personnel and certified laboratories. Therefore, a highly sensitive and easy to use biosensor as a rapid detection method for foodborne pathogen is needed to ensure food safety and public health. The objective of this project was to design electrochemical biosensors based on the combination of platinum nanoparticles (n-Pt), pH-responsive polymer nanobrushes including, chitosan (CHI), alginate (ALG) and polyacrylic acid (PAA)), and aptamers for improved detection of *L. monocytogenes*. n-Pt was deposited onto electrodes using a pulsed sonoelectrodeposition (pulSED) method, which increased ($P < 0.05$) the electroactive surface area (ESA) from 0.018 ± 0.0004 cm^2 to 0.081 ± 0.0179 cm^2. Then, pH-responsive polymer brushes were electrodeposited onto the n-Pt. The optimized nanobrushes deposition increased ($P<0.05$) ESA to 0.101 ± 0.004 cm^2, 0.111 ± 0.012 cm^2, and 0.108 ± 0.022 cm^2 for CHI, ALG and PAA/n-Pt modified electrodes, respectively. Aptamers selective to *L. monocytogenes* were loaded onto the nanobrushes at 1000 nM, 400 nM, and 800 nM for CHI/n-Pt, PAA/n-Pt, and ALG/n-Pt electrodes, respectively. Loading aptamers onto the pH-responsive nanobrushes improved ($P < 0.05$) biosensors performance, as they were actuated to extend during the bacteria capturing step and contract during the sensing process. The developed biosensors were tested in buffer and

a food matrix against another Gram-positive bacteria (*Staphylococcus aureus*) and showed a wide detection range of 10^1-10^8 CFU/mL of *L. monocytogenes* in 17 min. The 1000-nM-aptamer/CHI/n-Pt biosensors provided the lowest average of limits of detection (LODs), 1.37 ± 1.50 CFU/mL with a sensitivity of 7.27 ± 1.10 (1/log(CFU/mL)) based on charge transfer resistance (R_{ct}) changes. Conversely, the 400-nM-aptamer/ALG/n-Pt biosensors provided the most consistent results with LODs of 6.10 ± 1.95 CFU/mL and sensitivity of 5.97 ± 0.90 (1/log(CFU/mL)) based on R_{ct} data, respectively. The combination of aptamers and pH-responsive nanobrushes on n-Pt provided enhanced sensing performance over other published biosensors without requiring addition of reagents or sample pre-incubation.

DEDICATION

To my family, my wife and my daughter Shadan.

ACKNOWLEDGEMENTS

I would like to thank my committee chair, Dr. Gomes, and my committee members, Dr. Castell and Dr. Taylor for their guidance, support and patient throughout my Master's degree program. I would like also to thank Dr. McLamore and his research group at the University of Florida for their guidance throughout the course of this research.

Also, I thank my research group for their support; Daniela, Shubhangi, Tres, Cicero, Rummy, Ahmad, Kevin and Jecori.

CONTRIBUTORS AND FUNDING SOURCES

Contributors

This work was supervised by a thesis committee consisting of Professors Gomes and Castell-Perez of the Department of Biological & Agricultural Engineering and Professor Taylor of the Department of Animal Science and Professor McLamore (external member) from the Department of Agricultural and Biological Engineering at University of Florida.

Funding Sources

Graduate student was supported by a fellowship from King Saud University, Saudi Arabia, and the thesis research project was funded by the National Science Foundation (NSF grant # 1512659-nanobiosensing).

TABLE OF CONTENTS

Page

LIST OF FIGURES

Page

Page

LIST OF TABLES

CHAPTER I

INTRODUCTION

Foodborne illness is a common public health concern. It is estimated that foodborne diseases cost the United States $77.7 billion and kill 3,000 people annually (Scharff, 2012). Over 250 types of foodborne diseases have been identified; most of these diseases are caused by microbial pathogens, including various bacterial and viral organisms (CDC, 2016a). One of the top three causes of death from foodborne illnesses in the United States is *Listeria monocytogenes* which has been found to survive over a wide range of temperature (<1-45°C) and pH (4.0 to 9.5), as well as 0.92 water activity (Melo, Andrew, & Faleiro, 2015; Scallan et al., 2011). Therefore, it is not surprising to be found in soils and fresh food products of plant or animal origin (Allerberger & Wagner, 2010).

Furthermore, *L. monocytogenes* has been reported in raw and inadequately pasteurized milk, soft cheeses, poultry, ready to eat food, fresh and frozen meat, and seafood as well as fruits and vegetables (Jay, Loessner, & Golden, 2008; Walderhaug, 2014). According to the Centers for Disease Control and Prevention (CDC) (2016b), recent listeriosis outbreaks have been linked to frozen vegetables, raw milk, packed salads, soft cheeses and ice cream. The infective dose of *L. monocytogenes* is undetermined; it depends on a variety of factors such as the food matrix involved and the strain and the host's health. For example, fewer than 100 cells in inadequately pasteurized milk may cause disease in individuals at high risk of infection (i.e.; older adults, newborns,

pregnant women, and individuals with weakened immune systems) (Walderhaug, 2014).

Current methods for foodborne bacteria detection, including *L. monocytogenes*, in food products are generally culture-based techniques, polymerase chain reaction, or immunoassays (Vanegas et al., 2016; Lazcka, Campo, & Muñoz, 2007). Although these conventional methods have proven their usefulness, they are laborious, requiring long time to receive confirmation, highly skilled personnel, and expensive/specific equipment (Sanvicens, Pastells, Pascual, & Marco, 2009). Therefore, there is a critical need for a rapid, accurate and easy-to-use method to detect foodborne pathogens such as *L. monocytogenes*.

Biosensors are analytical devices which convert a biological response into an electrical signal (Lee & Niederer, 2010), and they have shown promising results in many fields including the field of pathogen detection. This technology has the potential to provide reliable results in a much shorter time compared to conventional methods. Biosensors can be classified by the type of transducer: optical, electrochemical, thermometric, piezoelectric, and magnetic. Of these types, optical and electrochemical biosensors are the most prolific types in recent years (Lazcka et al., 2007). This research developed biosensors composed of metallic nanomaterials, pH-responsive polymer nanobrushes and DNA aptamers which distinguish this work from previously published biosensors. The combination of pH-responsive polymers with selective capture of bacteria by

aptamers immobilized on the polymer surface is expected to increase selective capture and retention of the target pathogens. When combined with nanomaterial-modified electrodes, this approach is expected to have two distinct advantages over other published biosensors: i) enhanced capture of target bacteria due to less non-specific binding, and ii) improved limit of detection and sensitivity.

CHAPTER II

LITERATURE REVIEW

Electrochemical biosensors are one of the fastest growing technologies in food analysis (Lazcka et al., 2007; Vidal et al., 2013). Electrochemical biosensors present significant advantages over other types of biosensors. The electrochemical sensors present high sensitivity and selectivity, inherent miniaturization, low cost, compatibility with novel microfabrication technologies, disposability, robustness, power requirements, simple-to-operate and independence of sample turbidity (Lazcka et al., 2007; Radi, 2011; Vidal et al., 2013). Due to these advantages, electrochemical biosensors are the possible alternative to conventional methods for pathogen detection (Lazcka et al., 2007; Vidal et al., 2013). The most common traditional electrochemical techniques used in biosensors are cyclic voltammetry, amperometry, potentiometry, and impedance spectroscopy (Grieshaber, Mackenzie, Vörös, & Reimhult, 2008).

Cyclic voltammetry (CV) provides information about the electrochemical reaction rates of analyte solutions and the redox potential. Three electrodes are used in the CV technique; working electrode, reference electrode and counter electrode (Grieshaber et al., 2008). CV is carried out by cycling the working electrode potential, and measuring the resulting current in the presence of a reference electrode which maintains a constant potential. The resulting applied potential provides an excitation signal in a triangular waveform as shown in Figure 1A. The potential extrema (point a on Figure 1A) is the point where the

voltage is sufficient to have caused a reduction or oxidation of an analyte and it is called switching potential (Grieshaber et al., 2008). A cyclic voltammogram obtained from a single electron oxidation and reduction is shown in Figure 1B (Kissinger & Heineman, 1983). Cyclic voltammogram of different electrode compositions is used to evaluate the electroactive surface area (ESA) by obtaining redox peaks of different scan rates in ferricyanide solution. Randles-Sevcik Equation (1.1) is used to calculate the ESA:

$$i_p = 2.69\text{x}10^5 \text{n}^{\frac{3}{2}} \cdot \text{A} \cdot \text{D}^{\frac{1}{2}} \cdot \text{v}^{\frac{1}{2}} \qquad \text{(Equation 1.1)}$$

where: i_p is the reduction peak (A), n is the transferred electrons from the redox couple (n=1), A is the electroactive surface area (cm^2), D is the diffusion coefficient (6.7×10^{-6} $cm^2 \cdot s^{-1}$), C is the working solution concentration (4 mol cm^{-3}), and $v^{1/2}$ is the scan rate (V s^{-1}) (Burrs et al., 2015; Taguchi et al., 2016; Vanegas et al., 2014).

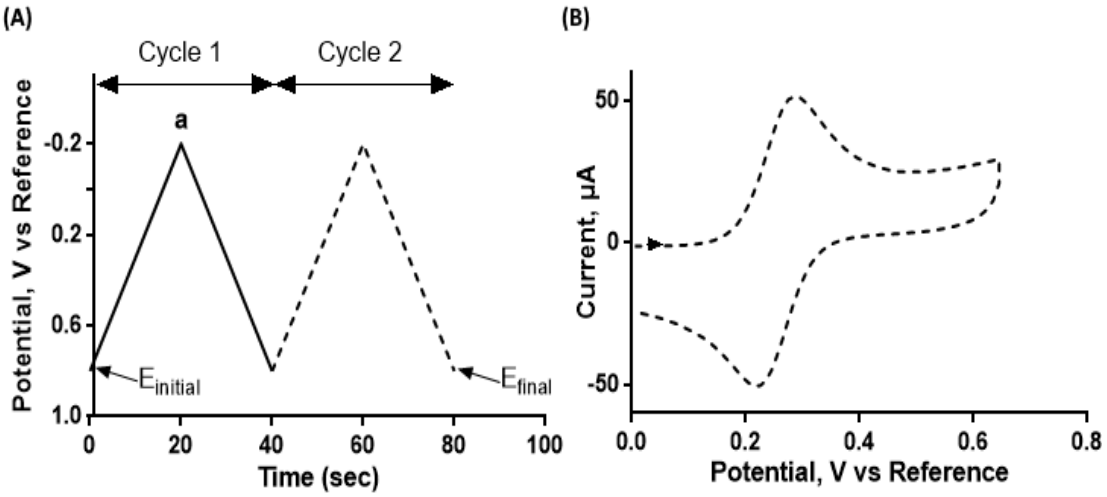

Figure 1: (A) Normal excitation signal for CV, a triangular potential waveform with switching potential at 0.8 and -0.2 V versus reference electrode. (B) Typical cyclic voltammogram of a single electron oxidation-reduction; ferrocyanide redox species, reprinted from Kissinger and Heineman (1983).

Electrochemical impedance spectroscopy (EIS) is a powerful and very sensitive technique which allows the study of the electrical properties in the development and analysis of sensing device transducers and trace the reactions occurring on it (Parkash & Skladal, 2008; Vidal et al., 2013). EIS is a useful technique to observe changes in electrical properties arising from biorecognition events occurring at the surface of a modified electrode (Grieshaber et al., 2008). EIS is commonly used in the detection of foodborne pathogen bacteria (Huang et al., 2010; Maalouf, Hassen, Fournier-Wirth, Coste, & Jaffrezic-Renault, 2008; Syed et al., 2011; Tan et al., 2011; Varshney & Li, 2007; Wan, Lin, Zhang, Wang, & Hou, 2011; Wan, Zhang, Wang, & Hou, 2010; Wang et al., 2009; Wang, Ruan, Kanayeva, Lassiter, & Li, 2008; Yang, Huang, Meng, Shen, & Jiao, 2009). However, to date, no reliable rapid sensors have been demonstrated in

field conditions for food safety applications that can to detect as few as 1 viable target cell in 25 g of food.

EIS is evaluated using either Bode or Nyquist plots. In the Bode plot (Figure 2C), total impedance $|Z|$ (Ω) is plotted against the logarithm of the excitation frequency (Hz) and in the Nyquist plot (Figure 2B), the imaginary impedance component Z" (Ω) is plotted against the real impedance component Z' (Ω) (Wang, Ye, & Ying, 2012). The physical interactions in the electrochemical cell between electrodes surface, solution and analyte can be interpreted by the Randles equivalent circuit model, shown in Figure 2A, a simple and commonly used equivalent circuit in EIS experiment analysis (Prodromidis, 2010). The circuit includes the resistance of the electrolyte R_s (Ω), the double layer capacitance C_{dl} (μF), the charge-transfer resistance R_{ct} (Ω) and Warburg impedance Z_w ($\Omega\ s^{1/2}$) (Prodromidis, 2010; Yang & Li, 2004)

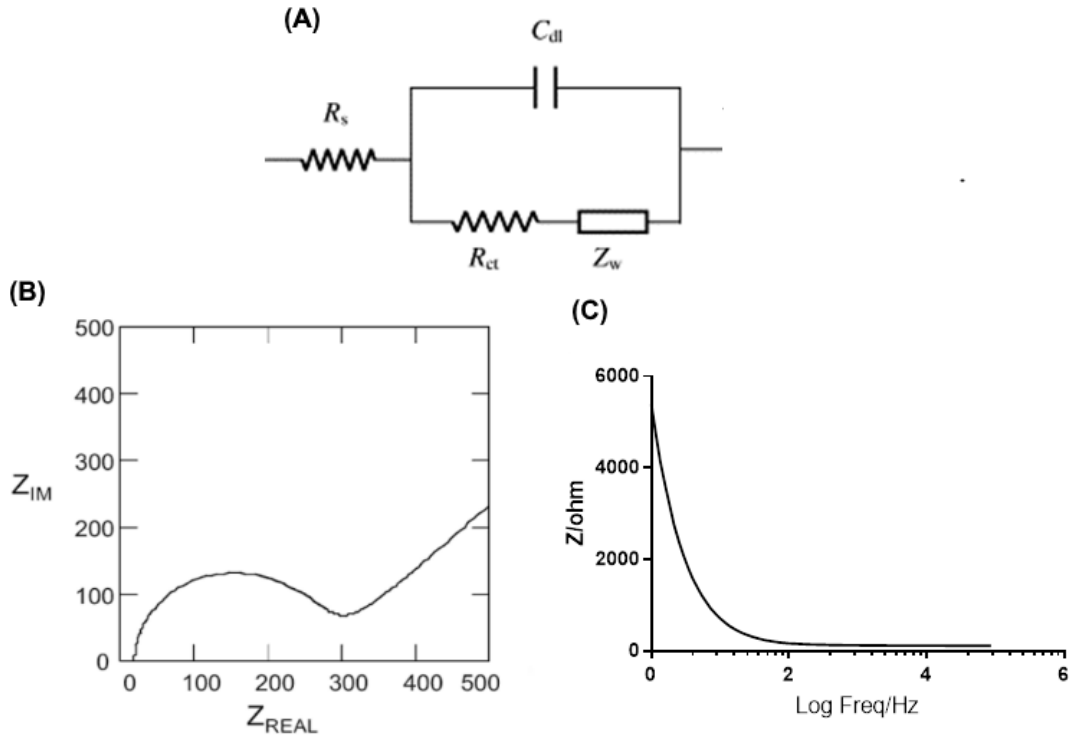

Figure 2: (A) Depiction of Randles equivalent circuit adapted from Yang and Li (2004). (B) Typical Nyquist plot of bare electrode and (C) Representative of Bode plot of bare electrode adapted from Lvovich (2012).

Biosensors are largely modified by conjugation of specific biorecognition elements such as aptamers and antibodies in order to improve the specificity of sensors to a particular analyte such as foodborne pathogen, heavy metals or drug residues (Sharma, Ragavan, Thakur, & Raghavarao, 2015). Aptamers are folded single-stranded nucleic acid or peptide molecules that can be natural or synthetic by origin (Grieshaber et al., 2008; Radi, 2011). Antibodies, or immunoglobulins (Ig) produced by the immune system, are large proteins that have high affinities and specificities for their target analytes (antigens). Although both aptamers and antibodies are used in biosensors development, aptamers

have several advantages over antibodies. The main advantages are that aptamers have equivalent and sometimes higher binding affinity towards their target analytes and are more thermal stability than antibodies. Another quality of aptamers is that they can be developed for almost any analyte while antibodies are limited. In addition, the smaller size of aptamers compared to antibodies results in lower limits of detection and higher sensitivities in biosensors (Crivianu-Gaita & Thompson, 2016).

Aptamers are generated by an *in vitro* selection process called SELEX (systematic evolution of the ligand by the exponential enrichment process). Briefly, from a large pool of sequences (usually $\approx 10^{15}$), a nucleotide sequence with high specificity towards a specific target (i.e., analyte) is selected based on affinity between the target and the aptamers. Aptamers are widely used as biorecognition elements in the modification of biosensors, with diagnostic kits based on electrochemical, chemiluminescence, piezoelectric principles and fluorescence (Sharma et al., 2015).

Table 1 shows several developed aptamers that capture *L. monocytogenes*. Suh, Dwivedi, Choi, & Jaykus (2014) and Lee et al.(2015) developed DNA aptamers that bind to more than one site on the cell of *L. monocytogenes* with high binding affinity. However, the developed aptamers were found to bind in considerable level to other bacteria including *Salmonella enterica, Bacillus cereus, L. grayi, L. innocua, Vibrio parahaemolyticus* and *Shigella sonnei.* Ohk, Koo, Sen, Yamamoto, & Bhunia (2010) developed aptamers that target internalin A, a surface protein, of *L. monocytogenes* with high selectivity. Moreover, these internalin A-sensitive aptamers have shown promising results when used in electrochemical biosensors for *L. monocytogenes* detection (Hills, 2016; Ohk et al., 2010; Sidhu et al., 2016; Sidhu, 2015).

Table 1: Summary of *L. monocytogenes* sensitive-aptamers.

Name	Selectivity	Sequence	Sequence Affinity (Kd, nM)	Structure	Bind To	Reference
LMCA2	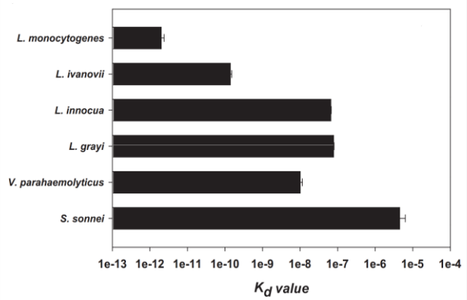	ATACCAGCTTATTCAATTCCAAAAGCGCACCCATATATGTTCTATGTCCCCCACCTCGAGATTGCACTTACTATCT	$2.01X10^{-3}$	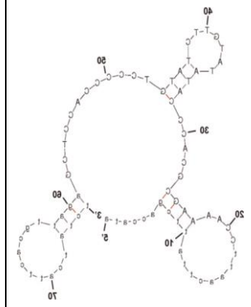	Unidentified cell surface site	(Lee et al., 2015)
LMCA26	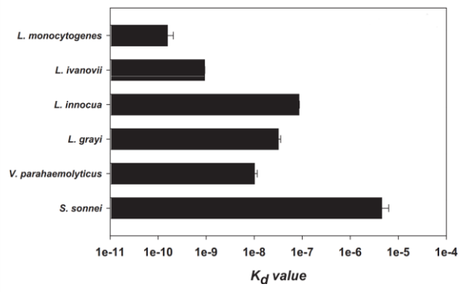	ATACCAGCTTATTCAATTCGATGGGGATTACTTATCATGAGAAACCAGCAGCATTTGAGATTGCACTTACTATCT	0.156	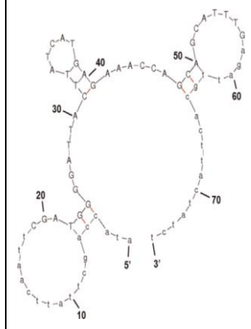	Unidentified cell surface site	(Lee et al., 2015)

Table 1: Continued

Name	Selectivity	Sequence	Sequence Affinity (Kd, nM)	Structure	Bind To	Reference
LM12-6	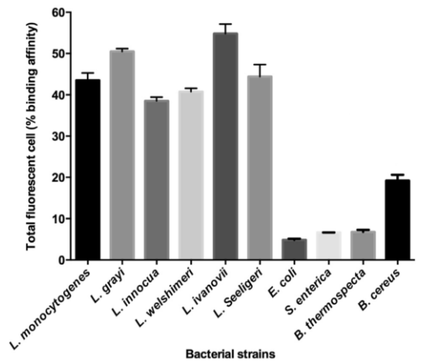	5'-TCTGTGTTCCGTTTTCGATTCTTACTGTGTTTTCGGGTGC-3'	106.4 ± 43.91	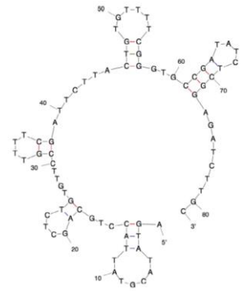	Unidentified cell surface site	(Suh et al., 2014)
InlA-aptamer	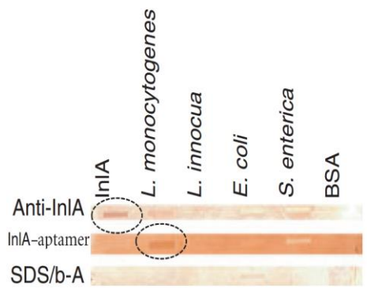	5'-ATC CAT GGG GCGGAGATGAGGGG GAGGAGGGCGGGTA CCCGGTTGAT-3'	Affinity constant of 10^3 CFU/mL	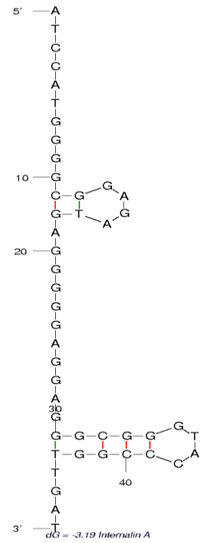	Internalin A protein	(Ohk et al., 2010)

Electrochemical aptasensors, biosensors based on aptamers, have been researched for detection of various chemical and proteins. However, there have been limited investigations on the detection of foodborne pathogens (Sharma & Mutharasan, 2013). A recent study involving the development of an electrochemical aptasensors to capture *L. monocytogenes* was able to achieve a 100 CFU/mL limit of detection in less than 3 hours (Vanegas et al., 2015). It is clear that there is a significant need to achieve a better limit of detection as well as develop rapid results to replace the current methods of detection.

Metallic nanoparticles are being gradually used as transducing materials in the fabrication of electrochemical biosensors for detection of food contaminants, toxins and pathogens analyses. Noble metal nanoparticles such as gold, silver and *platinum* are more advantageous than other nanomaterials due to ease of functionalization via simple chemistry, unique spectral and redox properties, high surface area-to-volume ratio, luminescence and conductivity properties (Sharma et al., 2015). Pulsed sonoelectrodeposition (pulSED) is a new technique for nanometals electrodeposition. This method combined two known deposition techniques, sonoelectrodeposition and pulse electrodeposition (Taguchi et al., 2016). The use of pulSED technique to deposit nanoplatinum (n-Pt) has been shown to improve the transducer conductivity for electrochemical biosensing (Taguchi et al., 2016). The use of the pulSED method forms not only a very small nanoparticles size (26.31 ± 1.3 nm) but also a homogenous, stable dendritic fractal structure. In addition, the pulSED technique uses small amounts

of platinum to form the structure of the transducer layer, subsequently reducing the costs of developing electrochemical biosensors (Taguchi et al., 2016).

Stimuli-responsive polymers are macromolecules with three-dimensional network structures that have received much attention in the biomedical and biological fields recently (Galaev & Mattiasson, 2001; Wan, Dai, Zhang, & Shen, 2015). These stimuli-sensitive polymers have the ability to exhibit significant changes in the swelling behavior of the network structure, mechanical strength and permeability as a result of changes in the environment. Slight variations in pH, temperature, ionic strength and electromagnetic radiation, for example, can cause rapid and reversible phase transitions from a hydrophilic to a hydrophobic structure (Galaev & Mattiasson, 2001). Most of the published studies of stimuli-responsive polymers have been conducted on either pH or temperature-sensitive materials (Ju, Kim, & Lee, 2001). pH-responsive polymers such as chitosan (CHI), alginate (ALG) and poly(acrylic acid) (PAA) have the ability to swell or shrink at pH values above or below their pK_a values based on their functional group (Jabbari & Nozari, 2000; López-León, Carvalho, Seijo, Ortega-Vinuesa, & Bastos-González, 2005).

Chitosan (poly-N-acetyl-d-glucosamine) is the one of the most abundant biopolymers in the world. The existence of the reactive hydroxyl and amino functional groups allow chitosan (CHI) to be easily modified by covalent functionalization, as shown in Figure 3A (Diaconu, Litescu, & Radu, 2010). CHI has a pK_a value between 6 and 7 depending upon the degree of deacetylation

and in basic solutions chitosan becomes uncharged and shrinks (López-León et al., 2005). Alginate or alginic acid is an inexpensive biodegradable polymer. Alginate (ALG) is an attractive polymer for fabrication of composite coatings by electrodeposition due to its linear structure with carboxyl end groups, as shown in Figure 3B (Cheong & Zhitomirsky, 2008). Alginate has an approximate pK_a value of 4 and 3.2 for mannuronic and guluronic acids, respectively, and swelling behavior occurs at a pH above the pK_a (Cook & Riley, 2012; Mallikarjuna Reddy et al., 2007). Poly(acrylic acid) (PAA) is a superabsorbent polymer of great interest in electrochemical, biomedical, electronic and optical devices applications (Wang, Deen, & Zhitomirsky, 2011). PAA is a homopolymer of acrylic acid with a carboxyl group on each monomer unit (every two carbon atoms) of the main chain, as shown in Figure 3C (Elliott, MacDonald, Nie, & Bowman, 2004; Terao, 2014). The presence of these carboxyl groups allows PAA to be functionalized by crosslinking reaction. PAA is reported to have an average pK_a value of 4.5 and swelling behavior at a pH above the pK_a (Jabbari & Nozari, 2000; Wiśniewska, Urban, Grząadka, Zarko, & Gun'ko, 2014).

CHI, ALG and PAA have been used in the design of biosensors as dispersion film (Lin, Lu, Ge, Cai, & Grimes, 2010; Mallikarjuna Reddy et al., 2007; Vidal et al., 2013; Wang & Anzai, 2015; Zhang et al., 2015) and a base to immobilize the biorecognition agent (Axelrod, Eltzov, & Marks, 2016; Burrs et al., 2015; Kurniawan, Tsakova, & Mirsky, 2006; Lin et al., 2010; Liu, Guo, Cui, & Yuan, 2009; Singh et al., 2013; Wan et al., 2015; Wang & Anzai, 2015; Zhang et

al., 2015). However, there are currently no studies in the literature, to the best of our knowledge, that have incorporated pH-responsive nanobrushes and used their actuation properties to enhance sensing performance of biosensors.

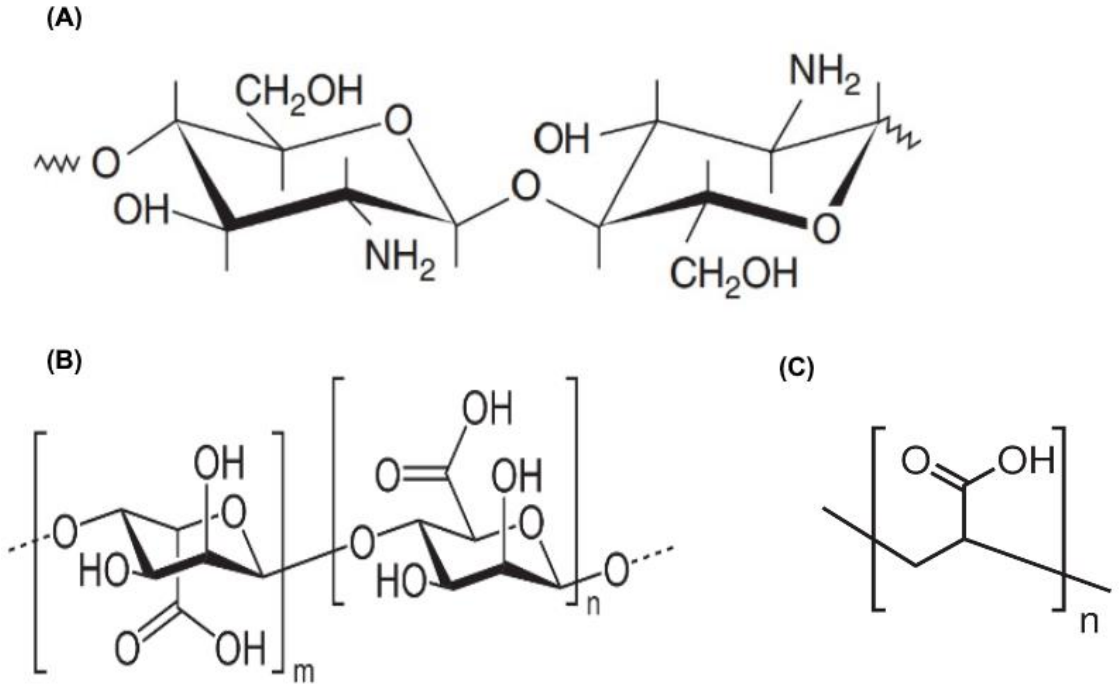

Figure 3: Chemical structure of (A) chitosan adapted from Belgacem and Gandini (2008),(B) alginate adapted from Chetia, Ansari, & Qureshi (2016), and (C) poly(acrylic acid) adapted from Wang et al. (2011).

The length and thickness of the polymer nanobrushes, i.e. grafted polymer chains, on the electrode surface can be controlled by an electrodeposition method (Wan et al., 2015). As the nanobrushes increase in length, their ability to load aptamers increase, which can improve the biosensor performance.

In addition, some polymers including CHI, ALG, and PAA are very porous materials, which improve the electron transfer resulting in increased sensitivity of the biosensor (Bhakta, Benavidez, & Garcia, 2014; Ju et al., 2001; Ma, Sun, & Hou, 2013; Medina, Nadres, Ballesteros, & Rodrigues, 2016). In addition, nanobrushes increase the biosensor surface area that interacts with the tested solution, subsequently increasing the likelihood of interaction between the analyte and the aptamers. This work developed aptasensors using electrodeposition method to fabricate the electrodes with platinum nanoparticles followed by the attachment of pH-responsive polymers using the same approach. Aptamers were then loaded on the polymer nanobrushes via chemical crosslinking reactions. The modified electrodes were tested to capture and quantify *L. monocytogenes*.

CHAPTER III

HYPOTHESIS AND OBJECTIVES

3.1 Hypothesis

Electrochemical detection of *Listeria monocytogenes* in complex food samples through the interaction between aptamers immobilized on pH-sensitive polymer hybrid nano-platinum platform with internalin A selective-aptamers will provide significant improvement in the sensing performance including the limit and range of detection, sensitivity, selectivity, and response time over the conventional methods and currently available biosensors.

3.2 Objectives

The main goal of this project was to design an electrochemical biosensor platform for real-time detection of *Listeria monocytogenes* composed of platinum nanoparticles, pH-responsive polymer nanobrushes and *Listeria monocytogenes* selective aptamers in a phosphate buffer solution (PBS) as well as a real-world scenario food product simulated by vegetable broth.

1 . Optimize platinum nanoparticles (n-Pt) deposition for the biosensor platform.
2. Optimize chitosan nanobrushes (CHI) deposition onto n-Pt electrode.
3. Optimize *L. monocytogenes* aptamers loading on n-Pt-CHI electrodes.
4. Determine the electrochemical response caused by the binding between aptamers and *L. monocytogenes* in order to define the biosensor

detection limit, range, sensitivity, selectivity, and response time.

5. Compare the changes in electrochemical response when substituting CHI for alginate and PAA.
6. Characterize the morphology of the nanomaterials on the modified electrodes using scanning electron microscopy (SEM).

CHAPTER IV

APTAMER-BASED BIOSENSOR FOR REAL-TIME DETECTION OF *LISTERIA MONOCYTOGENES* USING pH-RESPONSIVE POLYMER NANOBRUSHES AND METALLIC NANOPARTICLE PLATFORMS

4.1 Overview

Foodborne disease outbreaks caused by *Listeria monocytogenes* continue to present major public health concerns worldwide. Thus, the objective of this study was to design rapid, accurate, and sensitive electrochemical biosensors based on the combination of platinum nanoparticles (n-Pt), pH-responsive polymer nanobrushes including, chitosan (CHI), alginate (ALG) and polyacrylic acid (PAA)), and aptamers for improved detection of *Listeria monocytogenes*. n-Pt was deposited on electrodes using a pulsed sonoelectrodeposition (pulSED) method, which increased ($P < 0.05$) the electroactive surface area (ESA). Then, pH-responsive polymer brushes were electrodeposited onto the n-Pt. The optimized nanobrushes deposition further increased ($P<0.05$) ESA values to 0.101 ± 0.004 cm^2, 0.111 ± 0.012 cm^2, and 0.108 ± 0.022 cm^2 for CHI, ALG and PAA/n-Pt modified electrodes, respectively. Aptamers selective to *L. monocytogenes* were loaded onto the nanobrushes at 1000 nM, 400 nM, and 800 nM for CHI/n-Pt, PAA/n-Pt, and ALG/n-Pt electrodes, respectively. Loading aptamers onto the pH-responsive nanobrushes improved ($P < 0.05$) the biosensors performance as they were actuated to extend during the bacteria capturing step and contract during the sensing process. The

developed biosensors were tested in buffer and a food matrix against another Gram-positive bacterium (*Staphylococcus aureus*) and showed a wide detection range of 10^1-10^8 CFU/mL of *L. monocytogenes* in 17 min. The 1000-nM-aptamer/CHI/n-Pt biosensors provided the lowest average of limits of detection (LODs), 1.37 ± 1.50 CFU/mL and the 400-nM-aptamer/ALG/n-Pt biosensors provided the most consistent results with LODs of 6.10 ± 1.95 CFU/mL based on R_{ct} data, respectively. Overall, the combination of aptamers and pH-responsive nanobrushes on n-Pt provided enhanced sensing performance being among the most efficient capture mechanisms for *L. monocytogenes* and capable to cover the relevant levels for food safety analysis, without requiring addition of reagents or sample pre-incubation.

4.2 Introduction

Foodborne illness is a common public health concern. It is estimated that foodborne diseases cost the United States $77.7 billion and kill 3,000 people annually (Scharff, 2012). *Listeria monocytogenes*, the etiological agent of a highly fatal infection called listeriosis associated with the consumption of contaminated food, is one of the top three causes of death from foodborne illnesses in the United States and Europe (Allerberger & Wagner, 2010; Melo et al., 2015; Scallan et al., 2011). It has been found to grow under refrigeration temperatures, between pH 4.0 to 9.5 and 0.92 water activity (Melo et al., 2015; Scallan et al., 2011). *L. monocytogenes* is recognized as a major issue to public health authorities due to its case-fatality rate, 20-30 % affecting susceptible vulnerable population groups (e.g. children, pregnant women, elderly) and immunocompromised patients, and a high hospitalization rate (94%) (Allerberger & Wagner, 2010). Since the recognition of listeriosis as a foodborne illness in the 1980s, over 65 listeriosis outbreaks occurred in the U.S. and various food products have been involved in the transmission of the disease (CDC, 2016b).

Current commercial methods for the detection of foodborne bacteria in food products, including *L. monocytogenes,* are culture-based techniques, nucleic acid based assays and immunologically based methods (Vanegas et al., 2016; Lazcka, Campo, & Muñoz, 2007). Although these conventional methods have proven their usefulness, they are laborious, requiring long time to receive confirmation, highly skilled personnel, and expensive/specific equipment

(Sanvicens et al., 2009). Biosensors, particularly electrochemical sensors, are one of the fastest growing alternative techniques in food analysis due to their advantages, which include high sensitivity and selectivity, label-free, inherent miniaturization, low cost, compatibility with novel microfabrication technologies, disposability, robustness, power requirements, simple-to-operate and independence of sample turbidity (Lazcka et al., 2007; Radi, 2011; Vidal et al., 2013). This method of analysis has the potential to overcome the limitations of conventional techniques for pathogens detection. However, in food samples nearly all of these devices suffer from poor limit of detection (LOD), long response times (when including sample enrichment), and poor selectivity.

In biosensing, many groups have shown that the use of metallic nanostructures as transducer improve the performance of electrochemical biosensors (Burrs et al., 2016; Saha, Agasti, Kim, Li, & Rotello, 2012; Sozer & Kokini, 2009; Taguchi et al., 2016; Vanegas et al., 2014). Noble metal nanoparticles such as gold, silver and platinum are more advantageous than other nanomaterials due to ease of functionalization via simple chemistry, unique spectral and redox properties, high surface area-to-volume ratio, luminescence and conductivity properties (Sharma et al., 2015). Nanoplatinum particles have been deposited on a variety of sensing surfaces and shown to improve signal transduction, thereby potentially enhancing sensitivity, response time, and limit of detection (Badhulika, Paul, Rajesh, Terse, & Mulchandani, 2014; Burrs et al., 2016; Taguchi et al., 2016; Vanegas et al., 2014; Zhong et

al., 2012). Recently, a new nanoplatinum deposition method, using pulsed potential and sonication, i.e., pulsed sonoelectrodeposition (pulSED), has shown to deposit controlled nanostructures, allowing sensors surfaces to be tuned and consequently, increasing the electroactive surface area up to 14 times compared to unmodified electrodes, ultimately, improving electron transfer (Taguchi et al., 2016).

Stimuli responsive polymers have shown promising uses in the biomedical and biological fields recently (Galaev & Mattiasson, 2001; Wan, Dai, Zhang, & Shen, 2015). Polymers brushes are attractive for biosensors fabrication as they are tethered at one end and the rest of the polymer chain is readily available providing a stable platform for immobilizing biorecognition agents, in addition to increasing the surface area (Krishnamoorthy, Hakobyan, Ramstedt, & Gautrot, 2014; Tokareva, Minko, Fendler, & Hutter, 2004). These stimuli-sensitive polymers can exhibit significant changes in the swelling behavior of the network structure, mechanical strength and permeability as a result of changes in pH, temperature or ionic strength of the environment (Galaev & Mattiasson, 2001; Krishnamoorthy et al., 2014). pH-responsive polymers such as chitosan (CHI), alginate (ALG) and poly(acrylic acid) (PAA) are among the most studied type of stimuli-responsive polymers and they can swell or shrink at pH values above or below their pK_a values based on their functional group (Jabbari & Nozari, 2000; Ju et al., 2001; López-León et al., 2005). Moreover, stimuli responsive polymers, particularly pH responsive

polymers, have not been fully explored in biosensing applications.

Furthermore, there have been numerous biorecognition agents used to enhance selectivity for *L. monocytogenes* in complex samples such as food matrices (Bruno et al., 2015; Lee et al., 2015; Ohk, Koo, Sen, Yamamoto, & Bhunia, 2010; Suh & Jaykus, 2013). Aptamers are synthetic single-stranded DNA or RNA oligonucleotide that possess high recognition ability to specific target molecules, such as nucleic acids, proteins and cells (Luo, Liu, Xia, Xu, & Xie, 2014). Additionally, aptamers have many advantages such as high binding affinity, excellent controllability and easy production over other recognition elements (e.g. antibodies) (Crivianu-Gaita & Thompson, 2016; Wang et al., 2015). As a result, aptamers are widely used, as biorecognition elements, in the modification of biosensors, and diagnostic kits, based on electrochemical, chemiluminescence, piezoelectric principles and fluorescence (Sharma et al., 2015; Wang et al., 2015). Electrochemical aptasensors, biosensors based on aptamers, have been studied for detection of various chemical and proteins. However, there have been limited investigations on the detection of foodborne pathogens (Sharma & Mutharasan, 2013). To date, no reliable rapid sensors have been demonstrated in field conditions for food safety applications.

Here, we focus on combining the actuation of stimuli-responsive polymer nanobrushes immobilized on nanoplatinum with *L. monocytogenes* selective aptamers to significantly improve pathogens capture and sensing performance. We demonstrate rapid (< 20 min), label-free aptasensors for the detection of *L.*

monocytogenes based on pH-responsive polymer nanobrushes actuation and metallic nanoparticles platforms. First, platinum nanoparticles were electrodeposited onto platinum/iridium electrodes via pulSED technique followed by the electrochemical attachment of pH-responsive polymers namely chitosan, alginate and poly(acrylic acid). Both nanoplatinum and polymer nanobrush depositions were optimized before loading the modified electrodes with aptamers. Actuation tests were then conducted on the polymer-aptamer nanobrushes to determine the most efficient pathogen capture strategy. Finally, the nanobrush based biosensors were evaluated for *L. monocytogenes* capture and quantification over other Gram-positive cells in PBS buffer and in a food matrix.

4.3 Materials and methods

4.3.1. Chemicals and reagents

Chloroplatinic acid 8 wt. %, chitosan (low molecular weight, 75-85% deacetylated 20-300 cP, medium molecular weight, 75-85% deacetylated, 200-800 cP, and high molecular weight, > 75% deacetylated, 800-2000 cP), potassium phosphate monobasic, alginic acid sodium salt (low viscosity, 15-20 cP, medium viscosity, 5-40 cP, and high viscosity, 40-90 cP), sodium chloride, poly(acrylic acid) partial sodium salt solution, 61-65 wt. % (molecular weight ~2,000 g mol^{-1}) sodium phosphate dibasic, and 99.95% platinum wire (0.5 mm diameter) were purchased from Sigma-Aldrich Co. (St. Louis, MO).

Polycrystalline diamond suspensions (1 µm and 3 µm) and alumina slurry (0.05 µm) were obtained from Buehler (Lake Bluff, IL). Lead acetate ($Pb(C_2H_3O_2)_2$) (30% w/v) was purchased from Fisher Scientific (Pittsburgh, PA).

L. monocytogenes aptamers developed by Ohk et al. (2010) hat target Internalin A (47 DNA bases, $K_D = 10^3$ CFU/mL, Mw 14,991 g mol^{-1}) terminated at the 3' end with an amine group and similar aptamers terminated at the 3' end or with a thiol group were purchased from Gene Link Inc. (Hawthorne, NY). Commercially sterilized vegetable broth was purchased from a local grocery store (Kitchen Basics, Hunt Valley, MD). Platinum/iridium electrodes (Pt/Ir, BASi MF-2013, 1.6 mm diameter, 7.5 cm length), reference electrode (Ag/AgCl) and Pt auxiliary electrode were purchased from BASinc. (West Lafayette, IN). Tryptose phosphate broth (TPB) was bought from HiMedia (Mumbai, India). Tryptic soy broth (TSB), Tryptic soy agar (TSA), yeast extract, and buffered peptone water (BPW) were purchased from Becton, Dickson and Company (Sparks, MD). Sulfo-SMCC (sulfosuccinimidyl 4-(N-maleimidomethyl)cyclohexane-1-carboxylate) and EDC (1-ethyl-3-[3-dimethylaminopropyl]- carbodiimide) were purchased from ThermoScientific (Rockford, IL). Sulfo-NHS (N-hydroxysulfosuccinimide) was purchased from Biovision (Milpitas, CA). Potassium nitrate (KNO_3) was purchased from British Drug Houses (ON, Canada). MES (2-[morpholino]ethanesulfonic acid), alginic acid sodium salt (40-90 cP), and 1.5 mm diameter, 99.95% platinum wire were obtained from Alfa Aesar (St. Louis, MO). Tris EDTA (TE) buffer pH 7.4 was

purchased from Quality Biological (Gaithersburg, MD). Potassium ferricyanide trihydrate ($K_3FE(CN)_6$) were obtained from J.T. Baker (Phillipsburg, NJ).

4.3.2 Bacteria Cultures

Listeria monocytogenes (ATCC 15313) and *Staphylococcus aureus* (ATCC 25923) were resuscitated from frozen culture in TPB and TSB, respectively. All cells used two identical consecutive transfers and were incubated at 35°C for 24 hours under aerobic conditions and counts of revived cultures were collected in triplicate. Cultures were maintained on tryptic soy agar (TSA) and TSA with 0.6% yeast extract (TSAYE) slants for *S. aureus* and *L. monocytogenes*, respectively, and stored at 4°C for no more than 3 months. Samples of the bacteria were serially diluted in BPW and plated on TSA and TSAYE for *S. aureus* and *L. monocytogenes*, respectively. The samples were then incubated for 48 hours at 35 °C before counting the colony growth and reporting them as CFU/mL (Maturin & Peeler, 2015). *L. monocytogenes* and *S. aureus* are pathogenic microorganisms and must be handled using biosafety level 2 standards established by the National Institute of Health.

4.3.3 Nanoplatinum electrodeposition

Pt/Ir electrodes were initially polished and then modified with a nanoplatinum (n-Pt) transducer layer using the pulsed sonoelectrodeposition (pulSED) method described in Taguchi (2016). The pulSED system consisted of

a sonicator bath (42 kHz, Chicago Electric, Carol Stream, IL) and a DC power supply (Yorba Linda, CA) outfitted with a relay (Ningbo Single Relay Co, Ltd, China) and controlled by an Arduino Uno microcontroller (Spark Fun electronics, Niwot, CO). A custom MatLab program was used to control the duty cycle. Briefly, a 20-mL plating solution that contains 0.72% chloroplatinic acid and 0.001% lead acetate in a polyethylene terephthalate cup at 20°C was placed in the sonicator bath and the bath was filled with DI water. The tips of the Pt/Ir electrodes were surrounded with paper tape (Shurtape, Hickory, NC) prior to depositing n-Pt in order to prevent overgrowth. The hole on the tape was cut using a 2 mm-hole puncher (Pro-Master, Minden, NV). A 1.5 mm platinum wire and Pt/Ir electrode were connected to the anode and cathode of the power supply, respectively; and then were immersed into the plating solution. A constant overpotential of 10 V and plating time of 60-90 sec was used for the electrodeposition (Taguchi et al., 2016). The n-Pt modified electrodes were rinsed with DI water after the deposition and the tape removed.

4.3.4 Nanobrush electrodeposition

Chitosan (CHI) nanobrushes was electrodeposited on n-Pt electrodes using a DC power supply following procedure described in (Hills, 2016; Luo, Xu, Du, & Chen, 2004). To form chitosan (CHI) nanobrushes, a modified n-Pt electrode was connected to the DC power supply cathode with a 0.5 mm platinum wire as anode and immersed in 10 mL CHI solution (0.5% (w/v)). In

order to optimize nanobrushes sensing platforms different electrodeposition parameters were evaluated including polymer type and its molecular weight and concentration, and electrodeposition time and voltage, which were varied according to the polymer. For CHI nanobrushes, low (20-300 cP), medium (200-800 cP), and high (800-2000 cP) molecular weights were tested. The deposition voltage and time ranged from 1.75 to 2.25 V and from 2.5 to 10 min. Alginate (ALG) nanobrushes layer was deposited using the same set up of CHI deposition with the exception that the modified n-Pt electrode was connected to the anode and the 0.5 mm platinum wire to the cathode. Three ALG viscosity ranges were examined, 15-20 cP, 5-40 cP, and 40-90 cP, namely low, medium, and high viscosity, respectively. The initial optimization step of ALG was based on viscosity values because it is the closest reflection of the molecular weight of the macromolecule. The viscosity ranges were measured using 1% (w/v) ALG suspension in water. The ALG concentration, deposition voltage and deposition time ranged from 0.25 to 1.00 % (w/v), from 1 to 2 V and from 2.5 to 7.5 min, respectively (Wang et al., 2014). Similar set up to the ALG nanobrushes deposition was used for polyacrylic acid (PAA) nanobrushes deposition. PAA concentration, deposition voltage and deposition time were varied from 1.0 to 7.5 % (w/v), from 0.75 to 2.00 V, and from 2.5 to 10 min (Wang, Deen, & Zhitomirsky, 2011).

4.3.5 Morphology analysis

Scanning electron microscope (SEM) was used to analyze the morphology structure of the modified electrodes using a Quanta 600 FEG from FEI (Hillsboro, Oregon) at 5,000, 10,000 and 20,000 V and 720 to 33.000X magnifications. Electrodes were coated with a 10-nm thick layer of platinum using a Cressington sputter coater 208 HR (Watford, United Kingdom) and allowed to ventilate for 30 min prior to SEM imaging.

4.3.6 Aptamer immobilization

CHI/n-Pt electrodes were loaded with thiol-terminated aptamers using Sulfo-SMCC crosslinking reaction. The thiol modified aptamers were first reduced using dithiothreitol DTT reduction protocol provided by the manufacturer (GeneLink, 2011). Thiol-terminated aptamers were reconstituted in 27 µL Tris EDTA (TE) buffer to make a 100 µM thiol-terminated aptamers stock solution. Following, 5 mg Sulfo-SMCC was dissolved in 100 µL filtered water then diluted in 9.9 mL PBS (pH 7.2). Next, CHI/n-Pt electrodes were individually immersed in 500 µL of the Sulfo-SMCC solution and allowed to react for 1 hour at room temperature with periodic mixing. Then, the maleimide-activated CHI/n-Pt electrodes were rinsed with PBS and moved to a PBS solution (pH 7.2) containing thiol-terminated aptamers (either 250, 500, 750, 1000, or 1500 nM) for 1 hour with periodic mixing (Balamurugan, Obubuafo, Soper, & Spivak,

2008). Finally, the aptamer/CHI/n-Pt electrodes were rinsed and stored in PBS until further use.

ALG/n-Pt and PAA/n-Pt electrodes were modified with amine-terminated aptamers using EDC/Sulfo-NHS crosslinking reaction. First, the activation solution which consists of 2 mL MES buffer (pH 6.0, 0.1 M), 292.2 mg NaCl, 4 mg EDC, 11 mg sulfo-NHS and 8 mL ultrapure water was prepared. ALG/n-Pt and PAA/n-Pt electrodes were then individually placed in 500 µL of the activation solution for 50 min at room temperature. Next, the modified electrodes were removed from the activation solution and placed in PBS solution (pH 7.2) containing amine-terminated aptamers with concentrations ranging from 100 to 1500 nM for ALG/n-Pt electrodes, and from 100 to 1200 nM for PAA/n-Pt electrodes, for 2 hours under agitation (Balamurugan et al., 2008; Jantra et al., 2011). All aptamers modified electrodes were stored in PBS until further use.

4.3.7 Electrochemistry

All electrochemical impedance spectroscopy (EIS) and cyclic voltammetry (CV) tests were performed with a 3 electrode cell set up with a platinum auxiliary electrode and a Ag/AgCl reference electrode at room temperature using a CH Instruments potentiostat (CHI6044E; Austin, TX). CV test was conducted to determine the peak current and the electroactive surface area (ESA) in a 20-mL 4 mM $K_3Fe(CN)_6$/ 1 mM KNO_3 solution with a 10 sec quiet time, a 650 mV

switching potential and 50, 100, 150, and 200 mV·s^{-1} scan rates. The ESA was calculated using Randles-Sevcik Equation (4.1):

$$i_p = 2.69\text{x}10^5 \text{n}^{\frac{3}{2}} \cdot \text{A} \cdot \text{D}^{\frac{1}{2}} \cdot \text{v}^{\frac{1}{2}} \qquad \text{(Equation 4.1)}$$

where: i_p is the reduction peak (A), n is the transferred electrons from the redox couple (n=1), A is the electroactive surface area (cm^2), D is the diffusion coefficient (6.7 x 10^{-6} $cm^2 \cdot s^{-1}$), C is the working solution concentration (4 mol cm^{-3}), and $v^{1/2}$ is the scan rate (V s^{-1}) (Burrs et al., 2015; Taguchi et al., 2016; Vanegas et al., 2014). ESA percentage change is used in the optimization of polymer nanobrush deposition and it was calculated from Equation (4.2):

$$ESA\% = \left(\frac{ESA_{polymer} - ESA_{n-Pt}}{ESA_{n-Pt}} \right) \times 100 \qquad \text{(Equation 4.2)}$$

where: $ESA\%$ is the ESA percentage change. $ESA_{polymer}$ is the ESA of polymer nanobrushes/n-Pt modified electrode, ESA_{n-Pt} is the ESA of n-Pt modified electrode.

EIS was performed in a 20mL 4 mM $K_3Fe(CN)_6$/ 1 mM KCl solution with a frequency range of 1-100,000 Hz, AC amplitude of 100 mV and initial DC potential of 0.25 V (Burrs et al., 2015; Vanegas et al., 2014). The pH values for

the CV (4 mM $K_3Fe(CN)_6$/ 1 mM KNO_3) and EIS (4 mM $K_3Fe(CN)_6$/ 1 mM KCl) solutions were adjusted to pH 7.2 for n-Pt and CHI/n-Pt and to pH 3.5 for ALG/n-Pt and PAA/n-Pt, respectively. For the actuation tests, the pH of ferrocyanide solution was adjusted to pH 8 or pH 4 for CHI nanobrushes, and to pH 7.5 or pH 3.5 for ALG and PAA nanobrushes; respectively, using a 1 M HCl or NaOH solution; the pH of the ferrocyanide solution was monitored during tests to ensure reported pH did not change by more than 0.5 pH units. Resistance charge transfer (R_{ct}) was obtained using EIS data and the percentage change of R_{ct} is used to find the optimum aptamer concentration that can be loaded on polymer nanobrushes/n-Pt modified electrodes. R_{ct} % change is calculated using the following Equation (4.3):

$$R_{ct}\% = \left(\frac{R_{ct\ \ aptamer} - R_{ct\ \ electrode}}{R_{ct\ \ electrode}} \right) \times 100 \qquad \text{(Equation 4.3)}$$

where: $R_{ct}\%$ is the R_{ct} percentage change. $R_{ct\ \ aptamer}$ is the R_{ct} of aptamer/polymer-nanobrushes/n-Pt modified electrode, $R_{ct\ \ electrode}$ is the R_{ct} of polymer-nanobrushes/n-Pt modified electrode.

4.3.8 Bacteria Detection

EIS was used to determine the limit of detection (LOD), sensitivity, range of detection, and selectivity of biosensors when exposed to bacteria at

concentrations varying from 10^1-10^8 CFU mL^{-1}. Complex plane diagrams (Nyquist plots - imaginary impedance versus real impedance) were used to determine the solution resistance (R_s), charge transfer resistance (R_{ct}), Warburg impedance (Z_w), and double layer capacitance (C_{dl}). Bode plots (impedance versus frequency) were used to determine the impedance at a fixed cutoff frequency (Z). The limit of detection (LOD) for each biosensor was calculated from Equation (4.4):

$$LOD = \frac{3\sigma - b}{s} \qquad \text{(Equation 4.4)}$$

where the standard deviation (σ) is determined from repeated measurements of the change in impedance (ΔZ) or the change in R_{ct} in cell-free electrolyte (baseline), *b* is y-intercept of the linear calibration curve, and the slope of the calibration curve is (s) (Radhakrishnan, Jahne, Rogers, & Suni, 2013). Sensitivity to the target bacterium was measured as the slope of the linear portion of the calibration curve consisting of the change in normalized impedance (ΔZ_N) or change in charge transfer resistance (ΔR_{ctN}) vs. the log concentration of cells (log CFU/mL) (Vanegas et al., 2015). The change in normalized impedance (ΔZ_N) was determined from Bode plots using Equation (4.5), where Z_0 is the measured total impedance (Ω) of the aptamer modified

electrodes in the absence of bacteria (i.e., baseline impedance) and Z_c is the measured total impedance (Ω) at the concentration being tested.

$$\Delta Z_N = \left(\frac{Z_c - Z_0}{Z_0} \right) \times 100 \qquad \text{(Equation 4.5)}$$

Similarly, the charge transfer resistance (ΔR_{ctN}) was calculated using Equation (6), where R_{ct0} is the measured R_{ct} (Ω) of the aptamer modified electrodes in the absence of bacteria (i.e., baseline impedance) and R_{ctc} is the R_{ct} (Ω) at the concentration being tested.

$$\Delta R_{ct\,N} = \left(\frac{R_{ct\,c} - R_{ct\,0}}{R_{ct0}} \right) \times 100 \qquad \text{(Equation 4.6)}$$

4.3.9 Statistical Analysis

A completely randomized design was used with equal replications in this study. All experiments were performed in triplicate as independent experiments and results were expressed as mean ± standard deviation. Statistical analysis was performed using IBM SPSS Statistics 24 software. Differences between variables were tested using one-way analysis of variance ANOVA and statistical

significance was expressed at the $P < 0.05$ level; significantly different means were separated by the Tukey test.

4.4 Results

4.4.1 Optimization of Nanoplatinum electrodeposition

Cyclic voltammetry (CV) was performed in order to determine the optimum n-Pt deposition time using pulSED technique on bare electrodes with four different deposition times (120-180 sec) tested. Each of these treated electrodes demonstrated reversible redox couples in potassium ferrocyanide. Representative CVs are shown in Figure 4A at a scan rate of 100 mV/sec and switching potential of 650 mV. Figure 4B shows the average ESA for bare and each treated electrode. Taguchi et al. (2016) explained that increasing the plating time results in higher ESA due to the deposition of more nanoplatinum onto the electrode. The ESA of bare electrodes (0.018 ± 0.0004 cm^2) was significantly lower than n-Pt modified electrodes for all four plating times. Depositing platinum for 140 sec increased the ESA to 0.081 ± 0.0179 cm^2, approximately 349% ESA increase, compared to the bare electrode. As seen in Figure 4B, the ESAs of n-Pt electrodes that were deposited for 160 and 180 sec were the highest; however, the deposited platinum extended beyond the electrode's surface (overgrowth). Therefore, 140 sec plating time was selected as the optimum deposition time for the n-Pt layer. Oxidative and reductive

current peaks, shown in Figure 4A, for all four pulSED treatment times were significantly higher ($p < 0.0001$, $\alpha = 0.05$) than the bare electrode.

Taguchi et al. (2016) reported a higher ESA value (0.3 cm^2) when depositing n-Pt for 180 sec compared to this study (0.107 ± 0.0205 cm^2), using the same pulSED technique. This is likely due to the thicker Pt wire used in this work, which has more contact area with the deposition solution, consequently, higher conductivity and more metal deposition (Sarwate, 1993). This resulted in less controlled deposition overtime; therefore, some of the deposited metal was located outside the Pt/Ir surface, on the tape used to prevent overgrowth, and had no effect on the ESA value. Another study by Burrs et al. (2016) used the pulSED technique to deposit nanoplatinum on paper based electrodes decorated with graphene and reported an ESA of (0.29 ± 0.05 cm^2).This higher ESA value could be linked to the hybrid material used to build up the sensor's transducer and to the higher physical surface area (0.03 cm^2) compared to this work (0.02 cm^2).Whereas, Chaturvedi et al. (2014) achieved a lower ESA (0.029 ± 0.01 cm^2) using a traditional electrodeposition method, which did not incorporate pulsing and sonication in the process, to deposit nanoplatinum on Pt/Ir electrodes.

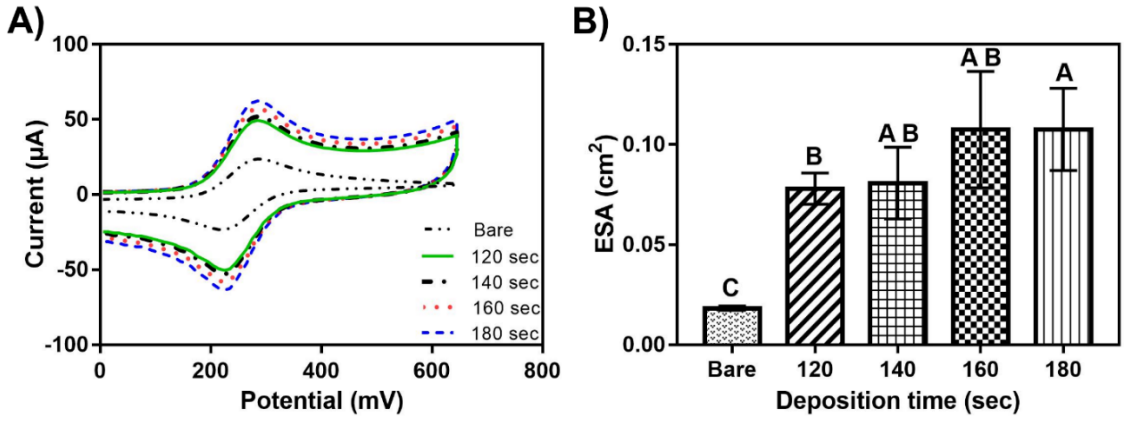

Figure 4: Optimization of nanoplatinum (n-Pt) deposition on bare electrodes. A) Representative cyclic voltammograms of bare and n-Pt modified electrodes over different deposition times (120-180 sec) in a 4 mM $K_3Fe(CN)_6$/ 1 mM KCl solution at 100 mV/s scan rates and switching potential of 650 mV. B) Average electroactive surface area of bare and different n-Pt deposition times using pulSED technique. The error bars denote the standard deviation (n ≥ 3). Different letters indicate significance at $P < 0.05$.

4.4.2 Optimization of polymer electrodeposition

4.4.2.1 Chitosan (CHI)

Optimization of chitosan nanobrush deposition on n-Pt electrodes was performed in three steps, optimizing molecular weight, deposition voltage, and deposition time. The representative CVs for each optimization steps are shown in Figure 5A-C. The shape of these CVs are characteristic of diffusion-controlled redox reactions, with well-defined redox peaks, which indicates that immobilization of chitosan onto the transducer did not alter the electrochemical behavior of the electrode. ESA percentage change was calculated using Equation (4.2).

Figure 5D-F shows the ESA % change for each optimization test. The change in ESA with different molecular weights of 0.5 % (w/v) chitosan (Figure

5D) showed that the highest and most consistent (i.e., reduced variance) increase in ESA was achieved from the low molecular weight (LMW) chitosan/n-Pt, which was also corroborated by the highest oxidative and reductive current peaks shown in Figure 5A. Next, the ESA of LMW CHI/n-Pt electrodes was measured, while varying electrodeposition voltage (1.75 to 2.25 V). As shown in Figure 5B & E, electrodepositing LMW CHI at 2 V provided the optimum deposition voltage. The third step was to vary the deposition time (2.5 to 10 min) and the highest and most consistent ESA increase was measured when depositing LMW CHI at 2 V for 5 min, as shown in Figure 5C & F. The electrodeposition of 0.5% (w/v) LMW chitosan for 5 min at 2 V on n-Pt electrode increased the ESA to (0.101 ± 0.004 cm^2). Figure 5G shows representative cyclic voltammograms at a 100 mV/s scan rate and switching potential of 650 mV for bare, n-Pt, and the optimized CHI/n-Pt electrodes. In this work, chitosan deposition showed to improve electron transport by significantly increasing the ESA values, contrary to Burrs et al. (2015), which reported a slight reduction in ESA value (approximately 0.05%) when depositing chitosan on platinum/graphene/platinum modified electrodes, and explained that the relatively high electron mobility in the platinum/graphene/platinum layer was the cause of the reduction. Furthermore, Burrs et al. (2015), used drop coating to deposit chitosan onto the electrodes, without any optimization.

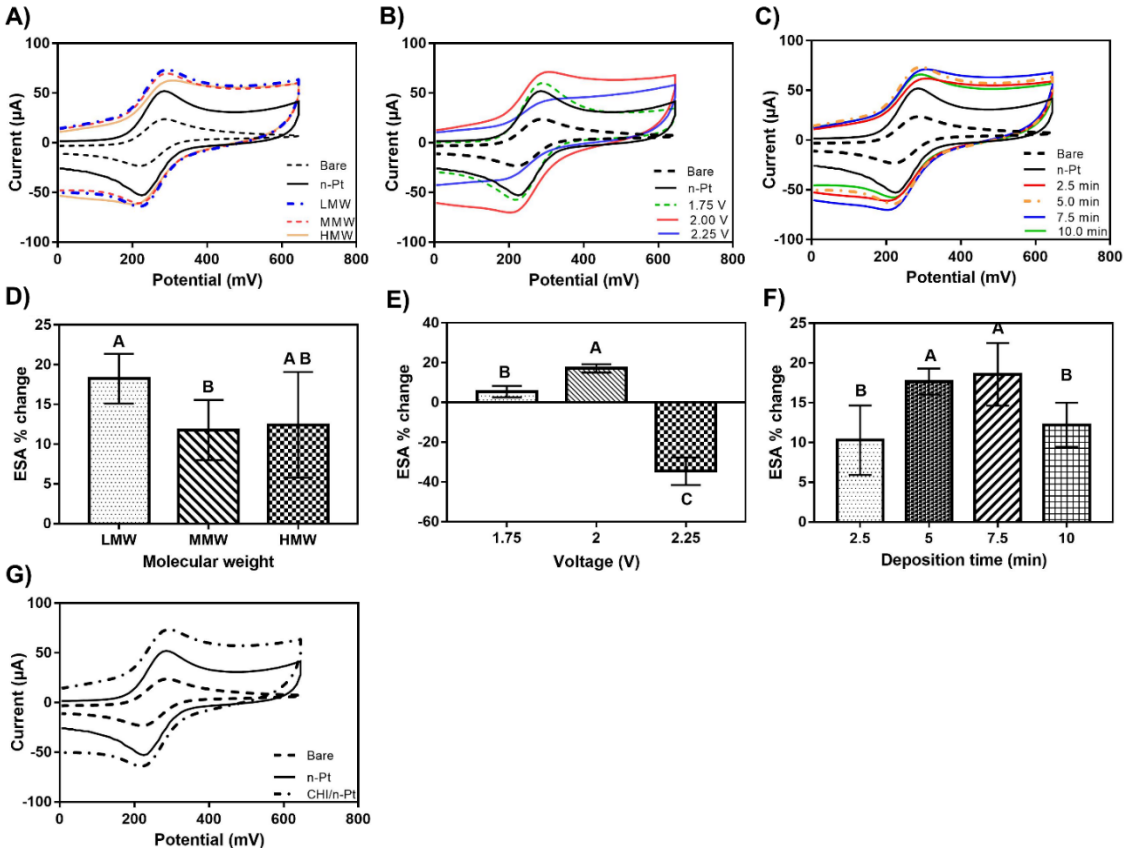

Figure 5: Optimization of chitosan (CHI) nanobrushes electrodeposition on n-Pt electrodes. Representative cyclic voltammograms in a 4 mM $K_3Fe(CN)_6$/ 1 mM KCl solution at 100 mV/s scan rates and switching potential of 650 mV of A) Bare, n-Pt, and low (LMW), medium (MMW) and high (HMW) molecular weights of CHI/n-Pt modified electrodes, 2 V deposition voltage and 5 min deposition time; B) Bare, n-Pt, and LMW CHI/n-Pt modified electrodes, 1.75 to 2 V deposition voltage and 5 min deposition time; and C) Bare, n-Pt, and LMW CHI/n-Pt modified electrodes, 2 V deposition voltage, and 2.5 to 10 min deposition times. D) Electroactive surface area (ESA) percentage change from CV analysis obtained at different molecular weights of 0.5% (w/v) chitosan (CHI), 5 min deposition time and 2 V deposition voltage. E) ESA percentage change obtained at different deposition voltage for 0.5% (w/v) LMW CHI and 5 min deposition time. F) ESA percentage change obtained at different deposition time for 0.5% (w/v) LMW CHI 2 V deposition voltage. G) Representative cyclic voltammograms in ferrocyanide solution at 100 mV/s scan rates and switching potential of 650 mV of Bare, n-Pt, and optimized CHI/n-Pt electrodes (LMW CHI, 2 V deposition voltage and 5 min deposition time). Error bars were based on the standard deviations ($n \geq 3$). Different letters indicate significance at $P < 0.05$. ESA % change was calculated using Eq. 4.2.

4.4.2.2 Alginate (ALG)

The optimum conditions for alginate nanobrush deposition on n-Pt electrodes was accomplished using four steps, optimizing viscosity, concentration, deposition voltage, and deposition time. Figure 6A-D and Figure 6E-H show the representative CVs and the ESA percentage changes for each optimization test, respectively. Each CV shape indicates a response characteristic of a reversible couple with clear redox peaks signifying that ALG had no negative impact on the electrochemical behavior of the electrode. Optimizing ALG viscosity resulted on finding that the change in ESA for low viscosity (LV) ALG was significantly higher than both medium and high viscosity (MV, HV) ALGs, as shown in Figure 6A and supported by Figure 6E. Next, the concentration of LV ALG was varied (0.25 to 1% w/v) and the highest ESA change of LV ALG/n-Pt electrodes was observed using 0.5% (w/v) LV ALG as shown in Figure 6B & F.

The deposition voltage was then optimized by measuring the ESA change of 0.5% (w/v) LV ALG/n-Pt electrodes when using three different deposition voltages (1 to 2 V). As shown in Figure 6C & G, the optimum deposition voltage was 1.5 V. The last step was to optimize the deposition time by varying the 0.5% (w/v) LV ALG deposition time (2.5 to 7.5 min) at 1.5 V deposition voltage, and 5 min of ALG deposition provided the highest ($P < 0.05$) increase in ESA (Figure 6D & H). The electrodeposition of 0.5% (w/v) LV ALG for 5 min at 1.5 V on n-Pt electrode increased the ESA to (0.111 ± 0.012 cm^2). Electrodeposition methods and electrochemical studies have been performed with alginate (Cheong & Zhitomirsky, 2008; Ozawa, Ino, Takahashi, Shiku, & Matsue, 2013; Wang et al., 2014) however, there are no studies reporting effects of alginate modified electrodes on ESA values nor electrochemical performance in the literature to compare our findings.

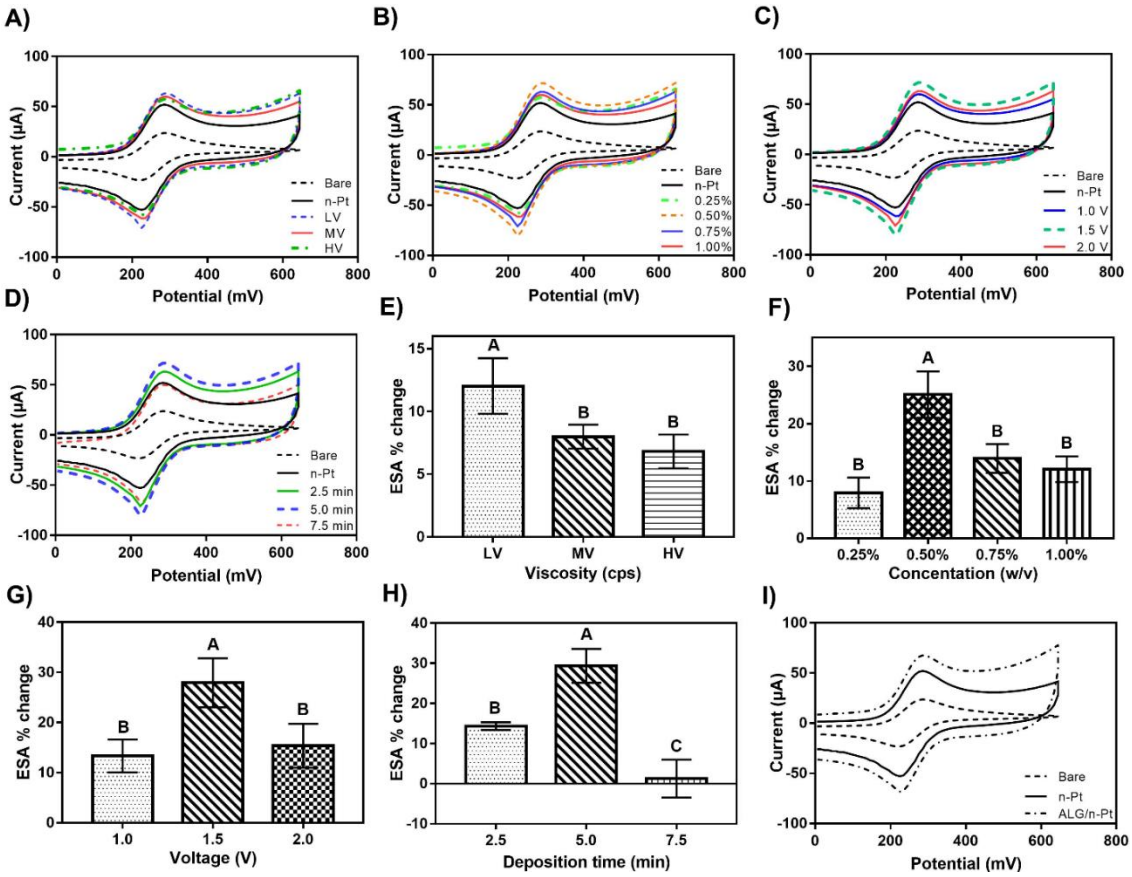

Figure 6: Optimization of alginate (ALG) nanobrush electrodeposition on n-Pt electrodes. Representative cyclic voltammograms in a 4 mM $K_3Fe(CN)_6$/ 1 mM KCl solution at 100 mV/s scan rates and switching potential of 650 mV of A) Bare, n-Pt, and low (LV), medium (MV) and high (HV) viscosities of ALG/n-Pt modified electrodes, 1.5 V deposition voltage and 5 min deposition time; B) Bare, n-Pt, and 0.25 to 1.00% (w/v) LV ALG/n-Pt modified electrodes, 1.5 V deposition voltage and 5 min deposition time; C) Bare, n-Pt, and 0.50% (w/v) LV ALG/n-Pt modified electrodes, 1.0 to 2.0 V deposition voltage and 5 min deposition time; and D) Bare, n-Pt, and 0.50% (w/v) LV ALG/n-Pt modified electrodes, 1.5 V deposition voltage and 2.5 to 7.5 min deposition time. E) Electroactive surface area (ESA) percentage change from CV analysis obtained at low (LV), medium (MV), and high (HV) viscosities of 1% (w/v) ALG using 5 min deposition time and 1.5 V deposition voltage. F) ESA percentage change obtained at different concentrations of LV ALG, 0.25 to 1.00% (w/v), using 1.5 V deposition voltage and 5 min deposition time. G) ESA percentage change calculated from depositing 0.50% (w/v) LV ALG for 5 min and three different voltages 1.0 to 2.0 V. H) ESA percentage change acquired from the deposition of 0.50% (w/v) LV ALG for different deposition time, 2.5 to 7.5 min, at 1.5 V deposition voltage. I) Representative cyclic voltammograms electrodes in ferrocyanide solution at 100 mV/s scan rates and switching potential of 650 mV of Bare, n-Pt, and the optimized LV ALG/n-Pt electrodes (0.50% w/v LV ALG, 1.5 V deposition voltage and 5 min deposition time). Error bars were based on the standard deviations ($n \geq 3$). Different letters indicate significance at $P < 0.05$. ESA % change was calculated using Eq. 4.2.

4.4.2.3 Polyacrylic acid (PAA)

Three optimization steps were used to identify the optimum electrodeposition conditions for PAA nanobrushes on n-Pt electrodes, optimizing concentration, deposition voltage, and deposition time. Figure 7A-C show the representative CVs for each optimization steps with similar CV shapes to CHI and ALG, indicating that immobilization of PAA onto the transducer had no impact on the electrochemical behavior of the electrode. The ESA % change for each optimization test are shown in Figure 7D-F. Optimizing the PAA concentration was performed by measuring the ESA % change of five different concentrations (1 to 7.5% w/v). As shown in Figure 7D, the ESA % change when electrodepositing 2.5% (w/v) PAA on n-Pt electrodes was significantly higher than the other concentrations, which was also supported by the highest oxidative and reductive peaks in Figure 7A.

Next, ESA of 2.5% (w/v) PAA/n-Pt electrodes was measured, while varying electrodeposition voltage (0.75 to 2 V) and it was clear that 1.5 V provided the highest ($P < 0.05$) increase in ESA as shown in Figure 7B & E. Four different deposition times (2.5 to 10 min) were then tested to identify the optimum time for deposition, as shown in Figure 7C & F. Overall, the highest ($P < 0.05$) and most consistent ESA increase was obtained from electrodepositing 2.5% (w/v) PAA for 5 min at 1.5 V. These optimum conditions increased the ESA of PAA/n-Pt electrodes to (0.108 ± 0.022 cm^2). Similar to alginate, there have been previous studies that electrodeposited PAA for different applications (De Giglio, Cometa, Cioffi, Torsi, & Sabbatini, 2007; Wang, Deen, & Zhitomirsky, 2011) other than electrochemical transduction. However, there is no published work reporting ESA values nor electrochemical performance of PAA modified electrodes to compare the observed results.

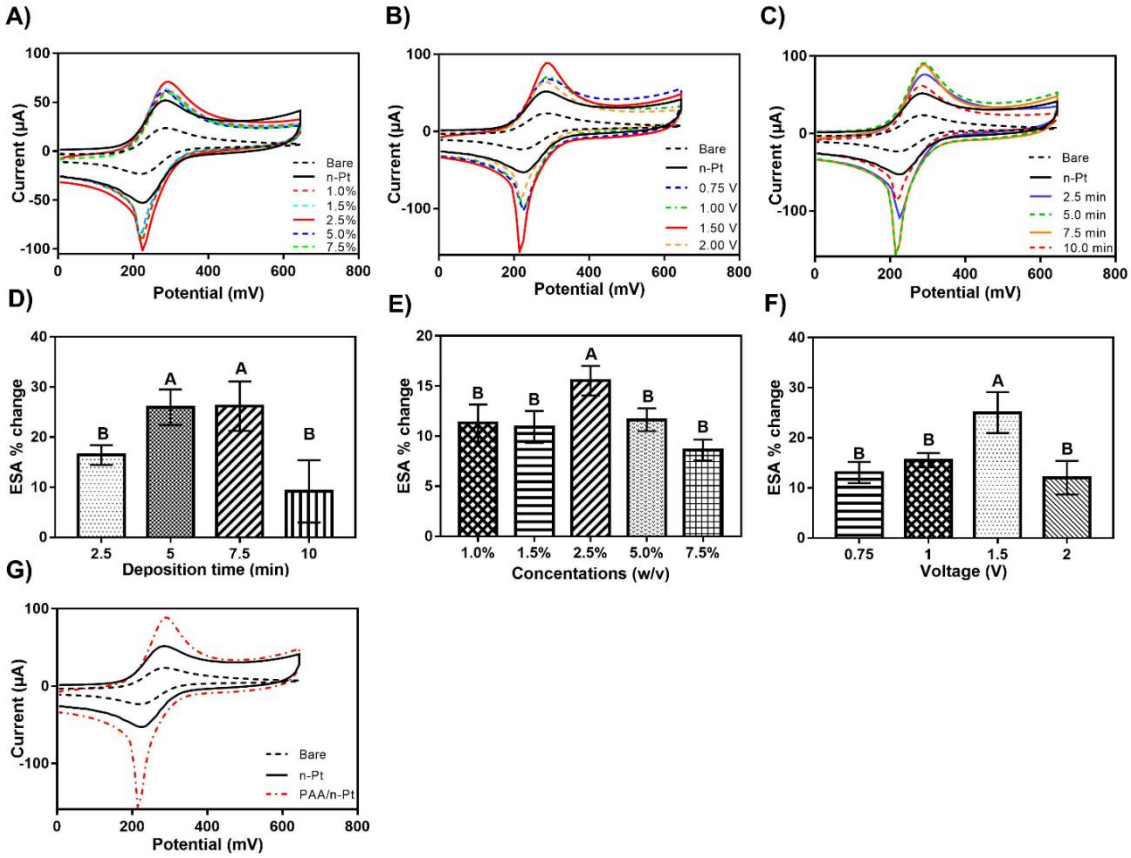

Figure 7: Optimization of polyacrylic acid (PAA) nanobrush electrodeposition on n-Pt electrodes. Representative cyclic voltammograms in a 4 mM $K_3Fe(CN)_6$/ 1 mM KCl solution at 100 mV/s scan rates and switching potential of 650 mV of A) Bare, n-Pt, and 1.0 to 7.5% (w/v) PAA/n-Pt modified electrodes, 1.0 V deposition voltage and 5 min deposition time; B) Bare, n-Pt, and 2.5% (w/v) PAA/n-Pt modified electrodes, 0.75 to 2.0 V deposition voltage and 5 min deposition time; C) Bare, n-Pt, and 2.5% (w/v) PAA/n-Pt modified electrodes, 1.5 V deposition voltage and 2.5 to 10 min deposition time. D) Electroactive surface area (ESA) percentage change from CV analysis obtained at concentrations of PAA 1.0 to 7.5% (w/v) using 1.0 V deposition voltage and 5 min deposition time. E) ESA percentage change calculated from depositing 2.5% (w/v) PAA for 5 min and different deposition voltages 0.75 to 2.0 V. F) ESA percentage change acquired from the deposition of 2.5% (w/v) PAA for different deposition time 2.5 to 10 min at 1.5 V deposition voltage. G) Representative cyclic voltammograms electrodes in ferrocyanide solution at 100 mV/s scan rates and switching potential of 650 mV of Bare, n-Pt, and the optimized PAA/n-Pt electrodes (2.5% w/v PAA, 1.5 V deposition voltage, and 5 min deposition time). Error bars were based on the standard deviations ($n \geq 3$). Different letters indicate significance at $P < 0.05$. ESA % change was calculated using Eq. 4.2.

4.4.3 Morphology analysis

The optimized n-Pt electrodes, CHI, ALG and PAA/n-Pt electrodes were subjected to SEM imaging, as shown in Figure 8. Figure 8A-C show the morphology of n-Pt electrodes showing to have nanocauliflower structures. Platinum nanocauliflowers ranged from 50 nm to 200 nm in particle size. The specific particles size of Pt nanocauliflower was not determined since it was noted by Kong et al. (2014) that cauliflower structures are inherently difficult to quantify. Pt nanocauliflowers structures was reported by Burrs et al. (2016) and Taguchi et al. (2016) when using the pulSED method with duty cycle of 500 mHz at 10 V for 140 sec. The SEM image shows homogeneous distribution of the nanoparticles with low variability.

Figure 8D-F show the optimized CHI/n-Pt electrodes with the Pt nanocauliflowers underneath a layer of CHI. The CHI layer was homogenously distributed across the surface and the layer followed the structural morphology of the nanocauliflowers underneath. The nanobrushes were not visible since the coated electrodes were dried before subjecting to SEM imaging and dried nanobrushes are assumed to be contracted or collapsed. Similarly, ALG/n-Pt electrodes showed individual brush-like structures that were consistently distributed covering most of the surface (Figure 8G-I). However, the structure had some brush-like clustered together. The size of individual ALG brushes ranged from 50 nm to 1 µm in diameter for clustered brushes. Figure 8J-L show the surface of the PAA/n-Pt electrodes. Similar to ALG coating, brush-like

structures were observed with slightly smaller size then ALG coating, diameter ranging from 25 nm for brushes to 600 nm for the clustered brush, respectively. It is difficult to compare both ALG and PAA deposition with published work (Cheong & Zhitomirsky, 2008; Ozawa, Ino, Takahashi, Shiku, & Matsue, 2013; Wang et al., 2014; Giglio, Cometa, Cioffi, Torsi, & Sabbatini, 2007; Wang, Deen, & Zhitomirsky, 2011) using similar electrodeposition methods since these previous work focused mostly on the thickness of the polymer layer evaluation than on their morphological characteristics. The PAA and ALG morphology are similar to Hills (2016), which electrodeposited CHI onto platinum/reduced graphene/platinum (PGP) creating finger/brush-like structure with a diameter of 250 nm to 500 nm. It is clearly seen that PAA coating were the least uniform coating across other polymers.

The morphological structures observed can be correlated with the ESA values results for the different platforms studied. For instance, the ESA values observed by CHI coating confirmed the homogeneous distribution of CHI coating, which resulted in very low variation on the ESA results (0.101 ± 0.004 cm^2). ALG and PAA had similar ESA values (0.111 ± 0.012 cm^2, and 0.108 ± 0.022 cm^2, respectively), which is also supported by their morphological characteristics. Moreover, PAA has the highest standard deviation when measuring ESA and that was corroborated by its structure being less uniform. CHI, ALG and PAA coatings increased ($P < 0.05$) the ESA values of the modified electrodes compared to n-Pt coating. These results are likely due to their electrochemical properties but also to the brush-like structure observed, increasing the surface area of the electrodes. The n-Pt electrodes seem to have a lighter coating of conductive material and consequently smaller surface area.

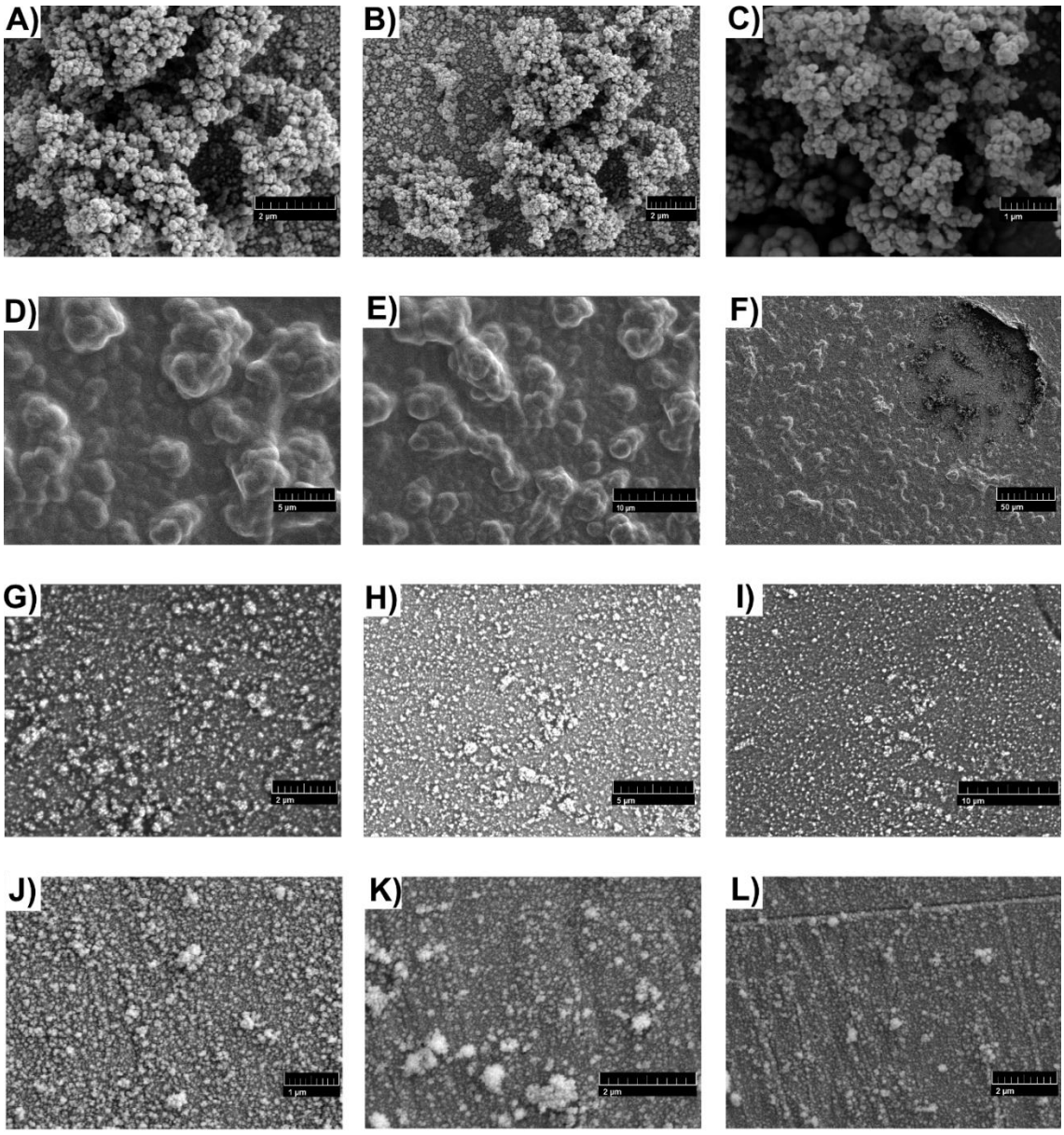

Figure 8: Morphology of optimized nanomaterial coatings obtained by Scanning Electron Microscopy (SEM). A-C) n-Pt modified electrodes obtained at 5,000 V and magnification of 24,900X, 15,100X and 23,000X, respectively; D-F) CHI/n-Pt electrodes obtained at 5,000 V and magnification of 7,590X, 5,020X and 720X, respectively; G-H) ALG/n-Pt/ electrodes obtained at 5,000 V and magnification of 20,000X, 10,000X and 6,240X, respectively; and J-L) PAA/n-Pt electrodes obtained at 10,000, 20,000 and 20,000 V and magnification of 33,800X, 29,900X and 20.100X, respectively.

4.4.4 Aptamer loading

Aptamer loading for all three-optimized polymer nanobrushes were determined using EIS analysis. Loading the highest amount of aptamers, to the saturation point, onto the nanobrushes increases the likelihood of capturing the target analyte, i.e.; *L. monocytogenes*) as well as improves sensor performance. Charge transfer Resistance (R_{ct}) was obtained from the EIS data using Zman software (WonATech Co.) simulated with the Randles equivalent circuit model shown in Figure 9G. The percentage change of R_{ct} at each concentration was calculated to define the optimum aptamer concentration that can be loaded onto the polymer nanobrushes using Equation (4.3). When aptamers are loaded the charge transfer resistance increases, therefore; the higher the positive R_{ct} change the more aptamer are loaded. The EIS data is also presented using the Nyquist plot, as shown in Figure 9D-F, which shows imaginary and real impedance values that reflect the capacitance and resistance of the electrochemical cell; respectively, over the entire range of frequency spectrum (1 Hz to 100 kHz) (Hunter, Mukundan, & Bhansali, 2008). Nyquist plots are usually represented by a semicircle region, which is normally observed at high frequencies corresponding to the R_{ct} and a straight line at lower frequencies corresponding to the mass transfer process (Pradeep, 2012).

CHI/n-Pt optimized electrodes were decorated with thiol-terminated aptamers using Sulfo-SMCC crosslinking reaction (Sapsford, Tyner, Dair, Deschamps, & Medintz, 2011). For CHI/n-Pt electrodes, the concentration of

1000 nM aptamer provided that highest ($P < 0.05$) percentage change in R_{ct} when loaded in CHI/n-Pt electrodes, shown in Figure 9A & D. ALG/n-Pt optimized electrodes and PAA/n-Pt optimized electrodes were grafted with amine-terminated aptamers using EDC/Sulfo-NHS crosslinking reaction (Sapsford et al., 2011). The concentration 400 nm and 800 nm showed the highest R_{ct} % change ($P < 0.05$), which represent the maximum loading of the bio-recognition element for ALG/n-Pt electrodes and PAA/n-Pt electrodes; as shown in Figure 9B-C & E-F, respectively. The maximum loading of aptamers for all the three nanobrushes modified electrodes varied considerably, which demonstrates that different platforms have different saturation points. This behavior has been reported in the literature. Vanegas et al. (2015) loaded the same aptamer, InlA aptamers (Ohk et al., 2010), onto hybrid nanomaterial platforms using a drop-casting method and reported increase in the resistance during the optimization of aptamer loading. Similarly, Sidhu et al. (2016) reported increase impedance when loading thiol-modified InlA aptamers onto platinum-interdigitated microelectrodes array using covalent adsorption and showed that 800 nM aptamers to be the optimum concentration. Erdem, Eksin, & Muti, (2014) fabricated chitosan/graphene/pencil graphite electrodes with anti-lysozyme DNA aptamer using EDC/Sulfo-NHS crosslinking reaction and reported that the R_{ct} increased as the aptamer concentration increased until it reached a saturation level.

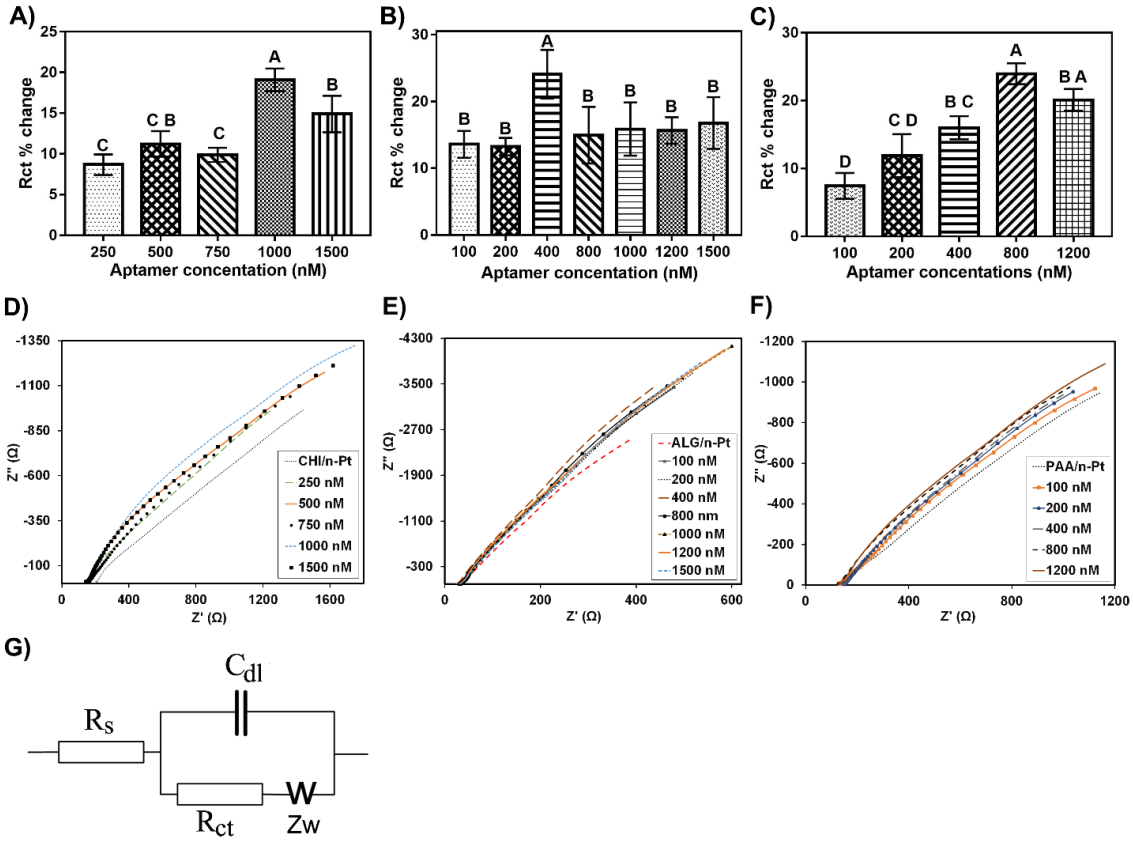

Figure 9: Resistance charge transfer (R_{ct}) percentage change resulted from immobilizing different aptamer concentrations on A) CHI/n-Pt, B) ALG/n-Pt, and C) PAA/n-Pt modified electrodes. Representative Nyquist plots for aptamer loading on D) CHI/n-Pt, E) ALG/n-Pt, and F) PAA/n-Pt modified electrodes at various concentrations obtained in a 4 mM $K_3Fe(CN)_6$/ 1 mM KCl solution at AC amplitude of 100 mV and initial DC potential of 0.25 V and a frequency range of 1-100,000 Hz. Z" is imaginary impedance in Ω and Z' is real impedance in Ω representing resistance and capacitance of the biosensor. G) Depiction of Randles equivalent circuit adapted from Yang and Li (2004). Error bars were based on the standard deviations (n ≥ 3). Different letters indicate significance at $P < 0.05$. R_{ct} % change was calculated using Eq. 4.3.

4.4.5 Polymer Actuation for Bacteria Capture

The actuation test was performed to study the reversibility of the polymer brushes and identify the optimum pHs for capturing and sensing the targeted bacteria, which was determined by the behavior of the nanobrushes configuration at certain pH conditions (i.e. extended or contracted) based on

their pKa. The initial test was carried out with aptamer/polymer/n-Pt electrodes in a 4 mM $K_3Fe(CN)_6$/ 1 mM KCl solution using CV analysis to identify the pH that produces the highest oxidation/reduction peaks (Figure 10A, E, and I). Subsequent tests using CV and EIS analyses in PBS in the presence of a known concentration (i.e., 10^2 CFU/mL) of *L. monocytogenes* were carried out to confirm the results obtained from the initial test, (Figure 10B-D, F-H, and J-L). Both tests were conducted at four different pH conditions, above and below the pK_a value of the tested polymer, for capturing and sensing steps.

Chitosan has a pK_a value between 6 and 7 with a predominantly positive charge at pH-values below 6 and in basic solutions chitosan becomes uncharged (López-León et al., 2005). Chitosan brushes showed a reversible behavior with the highest peak achieved from sitting the aptamer/CHI/n-Pt electrodes in a pH 4 ferrocyanide solution for 15 min and sensing with a similar solution at pH 8, as shown in Figure 10A. Although chitosan is not considered a highly conductive polymer, CV analysis in Figure 10A clearly shows the change in chitosan brushes electrical conductivity when pH changes (Khiar, Puteh, & Arof, 2006). This means that chitosan brushes contracted/shrank at pH 8 and reduced the resistance of the electrical flow in the system. When sensing in pH 4, the brushes extended/swelled resulting in increasing the resistance of electrical flow in the system. To confirm this finding, CV and EIS tests were performed in PBS in the presence of 10^2 CFU/mL of *L. monocytogenes* to test the capturing and sensing efficiency. Figure 10B-D show that capturing at pH 4

and sensing at pH 8 provided the highest peaks, impedance values, and change in R_{ct}. Cui et al. (2014) studied the swelling behavior and noted that when submerging chitosan in pH 1.2, the swelling ratio was much greater when at pH 7.4. The study by Burrs et al. (2015) concluded that pH 7.1 was the optimum condition for their electrochemical testing of chitosan modified biosensors. Therefore, pH 4 is the optimum condition to capture the targeted bacteria since chitosan brushes have higher contact area with the tested solution compared to pH 8 at which the brushes are contracted. In addition, the sensing process is best at pH 8 giving that the electrical flow is easier then at pH 4.

The actuation test of aptamer/ALG/electrodes was carried out in pH 3.5 and 7.5, considering that alginate is an acidic polymer that has a pK_a value of 4 to 3.2 (Mallikarjuna Reddy et al., 2007) Figure 10E shows representative CV curves at each pH conditions with the highest peak being achieved from sitting the electrodes at pH 7.5 and running the CV at pH 3.5. These results imply that alginate brushes have a reversible behavior and contract at pH 3.5 increasing the conductivity of the modified electrode. Conversely, the alginate brushes extend at pH 7.5 reducing the conductivity of the sensor. Figure 10F-H confirm the initial findings in the presence of bacteria in PBS by showing that the best electrochemical response (i.e., highest peaks, impedance values, and change in R_{ct}) was achieved from using pH 7.5 to capture and pH 3.5 to sense. Swelling behavior of alginate due to pH change has been noticed in other studies. For example, Pasparakis & Bouropoulos (2006) reported that the alginate shrink at

pH less than 4 due to the protonation of carboxylate groups of alginate. Shi et al. (2014) also noted that swelling ratio is considerably high in alkaline environment (pH 6.5) compared to acidic environment. Thus, pH 7.5 is the optimum condition for the bacteria capturing step and pH 3.5 is the optimum for performing the electrochemical testing/sensing.

Polyacrylic acid brushes on aptamer/PAA/n-Pt electrodes were tested in the same manner as alginate modified electrodes, since they have similar pK_a values, 4.5 and 4 to 3.2, respectively. Figure 10I shows a reversible behavior of the PAA brushes and the condition that provided the highest peak when running CV was sitting at pH 7.5 and testing at pH 3.5, which also demonstrates that PAA has limited electrical conductivity. More specifically, PAA brushes are extended at pH 7.5 and collapsed at pH 3.5, which allows for more contact with the solution tested, and for less resistance of electron flow in the system; respectively (Stamenkovic, Premovic, & Mentus, 1997). Testing with a fixed concentration of *L. monocytogenes* for all different conditions supported the initial results (i.e.; capturing at pH 7.5 and sensing at pH 3.5) by showing the best electrochemical response, as shown in Figure 10J-L and similar to the alginate results. The functional groups of PAA chains are carboxyl groups, which dissociate when the pH rises above the pK_a resulting in considerable swelling behavior (Jabbari & Nozari, 2000). Whereas, the PAA's functional groups are predominantly undissociated at pH below 4.5 exhibiting a shrinking behavior (Jabbari & Nozari, 2000; Wiśniewska et al., 2014). Therefore, the

optimum testing conditions for PAA modified electrodes are pH 7.5 for capturing the targeted analyte and pH 3.5 for conducting the electrochemical sensing.

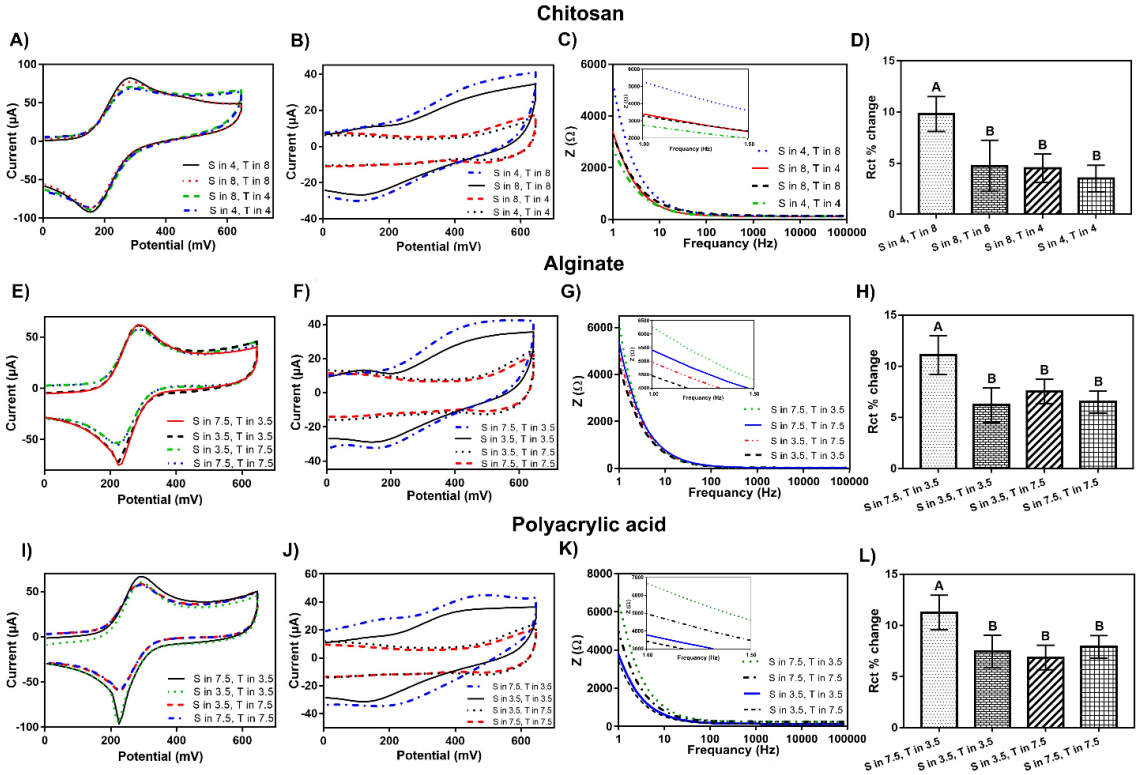

Figure 10: Polymer actuation test results for CHI, ALG, and PAA/n-Pt electrodes functionalized with lnl A aptamer. S is the pH at which the modified electrodes sat for 15 min and T is the pH at which CV and EIS analysis were performed. A, E and I are representative cyclic voltammograms obtained in a 4 mM $K_3Fe(CN)_6$/ 1 mM KCl solution in various pH testing conditions at 100 mV/s scan rates and switching potential of 650 mV for aptamer functionalized CHI/n-Pt, ALG/n-Pt, and PAA/n-Pt electrodes; respectively. B, F and J are CV curves obtained in PBS containing 10^2 CFU/mL of *L. monocytogenes* at 100 mV/s scan rates and switching potential of 650 mV in different pH testing conditions for aptamer functionalized CHI/n-Pt, ALG/n-Pt, and PAA/n-Pt electrodes; respectively. C, G and K are Bode plots acquired in various pH testing conditions in PBS containing 10^2 CFU/mL of *L. monocytogenes* using aptamer functionalized CHI/n-Pt, ALG/n-Pt, and PAA/n-Pt electrodes; respectively. The insets show the impedance Z values below 1.5 Hz. D, H, and L are charge transfer resistance (R_{ct}) percentage change resulted from capturing and sensing 10^2 CFU/mL of *L. monocytogenes* in PBS in different pH conditions using aptamer functionalized CHI/n-Pt, ALG/n-Pt, and PAA/n-Pt electrodes; respectively. All Bode plots obtained using EIS technique at AC amplitude of 100 mV and initial DC potential of 0.25 V and a frequency range of 1-100,000 Hz in PBS. Error bars were based on the standard deviations ($n \geq 3$). Different letters indicate significance at $P < 0.05$. R_{ct} % change was calculated using Eq. 4.3.

4.4.6 Characterization of Biosensors

Figure 11A-B were obtained from running EIS analysis for aptamer/CHI/n-Pt biosensor in PBS while increasing *L. monocytogenes* concentration. The inset in both figures show that *L. monocytogenes*- aptamer binding resulted in increased impedance at lower frequencies (below 10 Hz) as the bacteria concentration was increased. The direction of increasing frequencies on the Nyquist plot is from the right to left in Figure 11B. The impedance values at higher frequencies (above 10 Hz) in Figure 11A-B showed similar patterns, which overlapped depending on bacteria concentration, whereas lower frequencies (below 10 Hz) the impedance values consistently increased as the concentration of the bacteria increased. Similar behavior was observed when detecting *L. monocytogenes* in the presence of interference (*S. aureus*) and in a real food sample (Figure 11D, E, G and H). In addition, biosensors fabricated with ALG and PAA brushes followed the same pattern for all testing conditions (Figure 12A, B, D, E, G and H and 13A, B, D, E, G and H). Therefore, the total impedance values (Z) at 1 Hz and R_{ct} values were used to determine biosensor performance's parameters, i.e., limit range of detection, sensitivity, selectivity, and detection time. The response time for all sensing performance tests was 17 min, including 15 min for capturing and 2 min for sensing.

The 1000-nM-aptamer/CHI/n-Pt biosensors performance was initially measured in PBS. The total impedance (Z) and R_{ct} changes caused by the bacteria were found to increase linearly with the number of bacterial cell present

in the solution (Figure 11C-F). The limit of detection (LOD) along with the other performance parameters were calculated using both the Z and R_{ct} change shown on Table 2. The 1000-nM-aptamer/CHI/n-Pt biosensors provided a LOD of 4.37 ± 0.86 and 3.75 ± 0.50 CFU/mL based on Z and R_{ct} change, respectively, with a range of detection from 10^1 to 10^8 CFU/mL. The test was repeated in the presence of interference, i.e. *S. aureus* in PBS to examine the selectivity of the biosensor. The results were similar to *L. monocytogenes* sensing without interference with LODs of 6.10 ± 3.90 and 3.67 ± 3.34 CFU/mL based on Z and R_{ct} change, respectively (Figure 11C, D, E and F), and demonstrates the high selectivity of the aptamers. Further tests were conducted in vegetable broth to examine the 1000-nM-aptamer/CHI/n-Pt biosensor in a real food matrix (Figure 11G-H). The results showed a lower LOD when using R_{ct} data, 1.37 ± 1.50 CFU/mL (3.36 ± 1.46 CFU/mL using Z data). The reduction of LOD in a more complex medium could be a result of Brownian motion, which causes random movements to the molecules in the testing environment, consequently increasing the likelihood of bacterial cells-aptamers interaction (Hida, 1980). The same behavior of achieving lower LOD when testing in a complex medium was observed by Huang et al., (2015), who developed a dynamic light scattering (DLS) immunoassay using gold nanoparticles (GNP) for the detection of *L. monocytogenes* and achieved LOD of 35 and 22 CFU/mL in PBS and in sample of lettuce homogenized in water, respectively.

The sensitivity of 1000-nM-aptamer/CHI/n-Pt biosensors was calculated using the normalized Z and R_{ct} changes (Figure 11C, F and I). There was no significant difference ($P > 0.05$) in sensitivity between sensing *L. monocytogenes* in PBS and in the presence of *S. aureus,* as shown in Figure 11C-F, which corresponded to 14.57 ± 2.24 and 18.25 ± 3.00 (1/log(CFU/mL)) when using R_{ct} data, and 9.05 ± 1.55 and 10.64 ± 1.22 (1/log(CFU/mL)) when using Z data, respectively. However, the sensitivity dropped when testing in a complex medium, i.e. vegetable broth (Figure 11I). The results imply that the biosensors' selectivity can be impacted as the testing medium become more complex.

In order to evaluate the binding effectiveness of aptamers on the biosensors performance *L. monocytogenes* at increasing concentrations were exposed to CHI/n-Pt sensors in the absence of aptamers in PBS. The results revealed LODs of 24.61 ± 5.43 and 21.08 ± 6.32 CFU/mL with sensitivity of 5.86 ± 1.17 and 5.56 ± 1.64 (1/log(CFU/mL) based on normalized Z and R_{ct} change, respectively (Figure 11J). These results show that *L. monocytogenes* cells could attach to the CHI nanobrushes; however, the LODs were about four times higher than 1000-nM-aptamer/CHI/n-Pt sensors, further demonstrating aptamer selectivity toward *L. monocytogenes*.

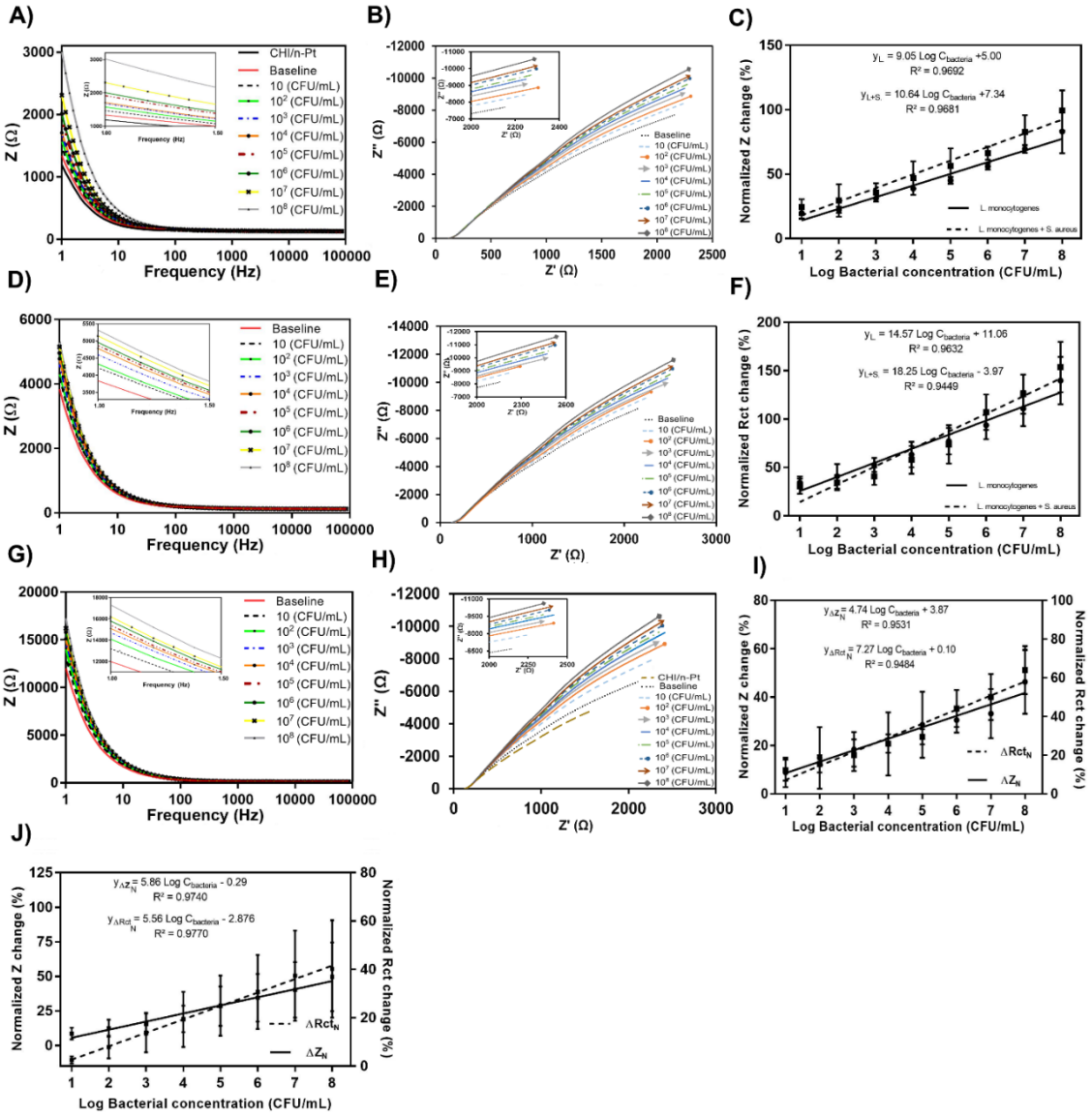

Figure 11: Detection of *L. monocytogenes* using 1000-nM-aptamer/CHI/n-Pt biosensors. Bacteria concentration ranged from 10^1 to 10^8 CFU/mL. A), D), and G) are Bode plots obtained from the detection of *L. monocytogenes* in PBS, in PBS in the presence of *S. aureus,* and in vegetable broth; respectively, the inset shows the impedance values at 1 Hz. B), E) and H) are Nyquist plots obtained from the detection of *L. monocytogenes* in PBS, in PBS in the presence of *S. aureus* and in vegetable broth, respectively, the inset shows the impedance values at 1 Hz. C) and F) are calibration curves for detecting *L. monocytogenes* alone and *L. monocytogenes* with *S. aureus*, in PBS plotted using normalized impedance (Z) and normalized charge transfer resistance (R_{ct}) change, respectively. I) and J) are calibration curves for detecting *L. monocytogenes* in vegetable broth and in the absence of aptamers in PBS, respectively, plotted using normalized Z change and normalized R_{ct} change. Error bars were based on the standard deviations (n ≥ 3). Normalized Z change and normalized R_{ct} change were calculated using Eq. 4.5 and 4.6, respectively.

Biosensors developed using 400-nM-aptamer/ALG/n-Pt were tested to sense *L. monocytogenes* following similar approach to 1000-nM-aptamer/CHI/n-Pt biosensors. As a result of increasing the bacteria concentration when testing 400-nM-aptamer/ALG/n-Pt biosensors, the impedance increased due to the aptamer-*L. monocytogenes* binding at lower frequencies (below 10 Hz) (Figure 12A-B). Hence, the total impedance values (Z) at 1 Hz and R_{ct} values were used to characterize the 400-nm-aptamer/ALG/n-Pt biosensors performance. Table 2 summarizes the biosensor performance's parameters, which had LODs of 1.17 ± 1.62 and 7.98 ± 1.72 CFU/mL in PBS based on Z and R_{ct} change, respectively. Slightly similar LODs were observed when testing in the presence of *S. aureus,* which confirms the selectivity of the biosensor, 4.76 ± 1.14 and 10.2 ±1.13 using Z and R_{ct} change, respectively. The performance of the 400-nM-aptamer/ALG/n-P biosensors in a food sample was carried out in vegetable broth (Figure 12G-H) and the LODs were 6.95 ± 1.63 and 6.10 ±1.95 CFU/mL using Z and R_{ct} change, respectively. The R_{ct} based LODs of 400-nM-aptamer/ALG/n-Pt biosensors had no statistical difference ($P > 0.05$) across all three-tested media. However, the Z based LOD in vegetable broth was significantly higher ($P < 0.05$) than LOD in PBS. The Z based LOD showed no significant difference ($P > 0.05$) when testing in PBS and when testing in the presence of interference. Based on R_{ct} data, it can be observed that the 400-nM-aptamer/ALG/n-Pt biosensors have high selectivity toward *L. monocytogenes* in the tested media. The sensitivity of 400-nM-aptamer/ALG/n-P biosensors was calculated using the normalized Z and R_{ct}

changes in three media, PBS, PBS with interference (*S. aureus*) and vegetable broth (Figure 12C, F and I).

The highest sensitivity was found when detecting *L. monocytogenes* alone in PBS, corresponding to 27.98 ± 3.15 (1/log(CFU/mL)) for normalized Z change, and 7.24 ± 0.91 (1/log(CFU/mL)) for normalized R_{ct} changes (Figure 12C-F). The sensitivity declined as the media become complex and became the lowest in vegetable broth 22.83 ± 1.84 and 2.82 ± 0.90 (1/log(CFU/mL) using normalized Z and R_{ct} changes, respectively (Figure 12I).

The role of aptamers was established in this biosensor by detecting *L. monocytogenes* in PBS using ALG/n-Pt sensors, i.e., without aptamers. The LOD was 50.92 ± 13.60 and 74.88 ±15.1 CFU/mL using Z and R_{ct} changes, respectively and the sensitivity was 13.46 ± 1.27 and 3.83 ± 0.55 (1/log(CFU/mL) using normalized Z and R_{ct}, respectively. Although the LOD showed that bacteria is being captured by the ALG brushes using ALG/n-Pt sensors, the LOD was significantly ($P < 0.05$) lower when capturing using 400-nM-aptamer/ALG/n-Pt sensors. Moreover, the sensitivity of ALG/n-Pt sensor was significantly lower ($P < 0.05$) than 400-nM-aptamer/ALG/n-P sensors in PBS detection (Figure 12C and J). Thus, these results demonstrate the selectivity of the aptamers toward *L. monocytogenes*, significantly enhancing the performance of the sensors fabricated with ALG brushes.

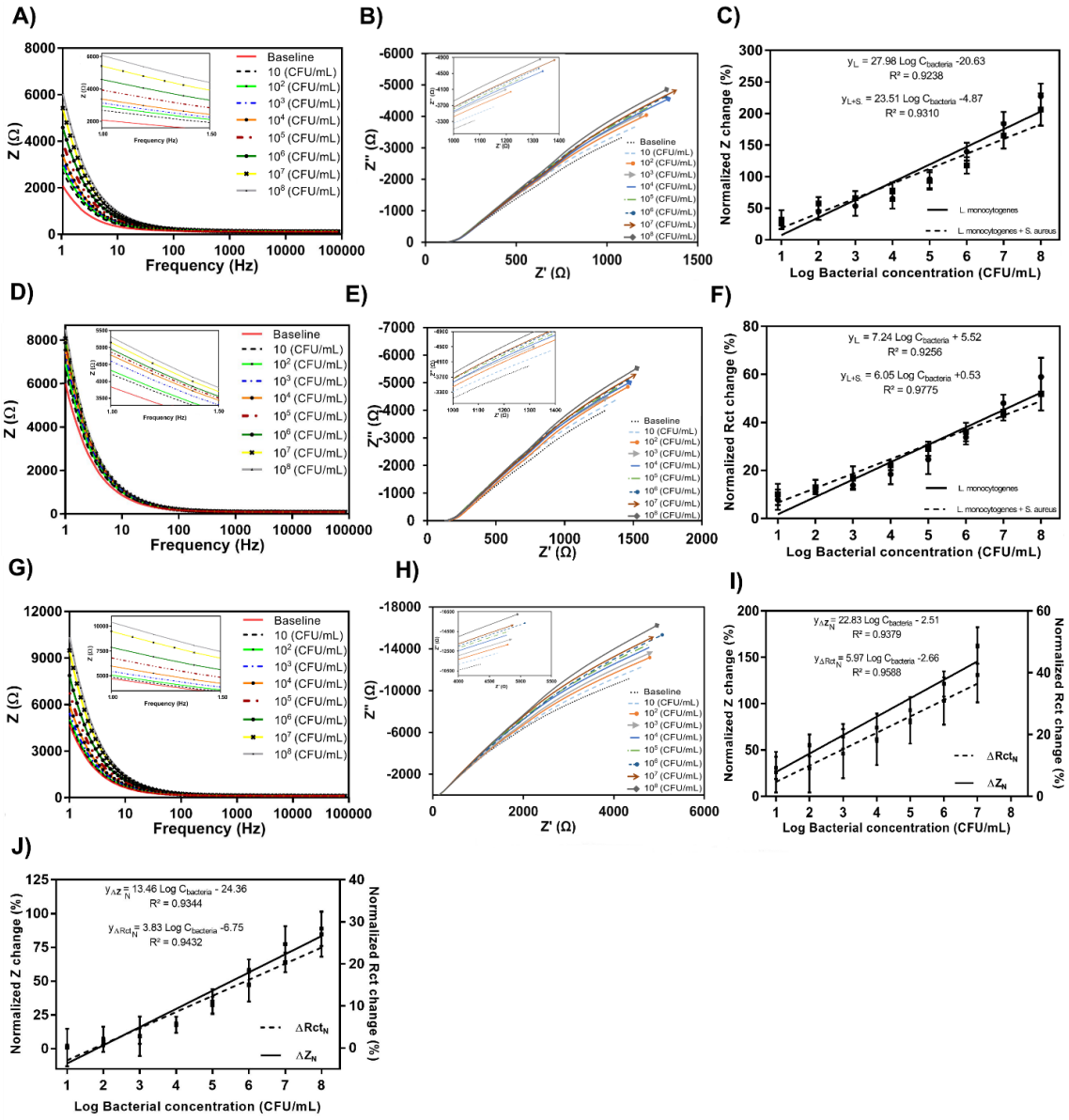

Figure 12: Detection of *L. monocytogenes* using 400-nM-aptamer/ALG/n-Pt biosensors. Bacteria concentration ranged from 10^1 to 10^8 CFU/mL. A), D), and G) are Bode plots obtained from the detection of *L. monocytogenes* in PBS, in PBS in the presence of *S. aureus,* and in vegetable broth, respectively, the inset shows the impedance values at 1 Hz. B), E), and H) are Nyquist plots obtained from the detection of *L. monocytogenes* in PBS, in PBS in the presence of *S. aureus,* and in vegetable broth, respectively, the inset shows the impedance values at 1 Hz. C) and F) are calibration curves for detecting *L. monocytogenes* alone and *L. monocytogenes* with *S. aureus*, in PBS plotted using normalized impedance (Z) and normalized charge transfer resistance (R_{ct}) change, respectively. I) and J) are calibration curves for detecting *L. monocytogenes* in vegetable broth, and in the absence of aptamers in PBS, respectively, plotted using normalized Z change and normalized R_{ct} change. Error bars were based on the standard deviations (n ≥ 3). Normalized Z change and normalized R_{ct} change were calculated using Eq. 4.5 and 4.6, respectively.

Biosensors modified with PAA brushes performance parameters were obtained based on Z and R_{ct} change, since they displayed similar behavior as CHI and ALG fabricated biosensors. The initial measurement of the 800-nM-aptamer/PAA/n-Pt biosensor performance's parameters was performed in PBS and revealed LODs of 5.90 ± 4.21 and 5.46 ± 4.70 CFU/mL using Z and R_{ct} change, respectively (Table 2, Figure 13A-B). This sensing platform was tested in the presence of *S. aureus* to examine the impact of interference, results showed LODs with no significant difference compared to LODs obtained without interference, and the LOD values corresponded to 3.72 ± 3.02 and 4.45 ±3.90 CFU/mL when using Z and R_{ct} change, respectively, (Figure 13D-E). Therefore, the presence of interference in PBS had no significant impact on 800-nM-aptamer/PAA/n-Pt biosensors performance. The biosensor was further tested in vegetable broth and the Z and R_{ct} changes showed LODs of 11.35 ± 3.16 and 8.35 ± 6.22 CFU/mL, respectively (Figure 13G-H). Similarly, there were no significant difference ($P > 0.05$) between LODs in PBS and vegetable broth. Thus, these results demonstrate that the 800-nM-aptamer/PAA/n-Pt biosensors is selective to capture and sense *L. monocytogenes* in different media.

The sensitivity of the 800-nM-aptamer/PAA/n-Pt biosensor was studied based on the normalized Z and R_{ct} changes (Figure 13C, F and I). R_{ct} based sensitivity values had no statistical significant difference ($P > 0.05$) in all the three media. However, the average value followed a slight reduction trend from 9.82 ± 2.29 (1/log(CFU/mL)) in PBS, then 7.32 ± 2.5 (1/log(CFU/mL)) in PBS in

the presence of interference, and 5.75 ± 1.85 (1/log(CFU/mL)) in vegetable broth. Similarly, Z based sensitivity had no significant ($P > 0.05$) difference between tests conducted in PBS and PBS with interference (13.61 ± 2.73 and 19.55 ± 3.47 (1/log(CFU/mL)), respectively). However, the Z based sensitivity value calculated from vegetable broth testing was significantly ($P < 0.05$) lower than the other two media (4.03 ± 2.07 (1/log(CFU/mL))). This means that the complex media can cause some interference that reduce the sensitivity.

The selectivity of aptamers on the biosensor performance was further analyzed by exposing increasing concentrations of *L. monocytogenes* to PAA/n-Pt sensors in the absence of aptamers in PBS. The LOD and sensitivity of PAA/n-Pt sensors were significantly ($P < 0.05$) different than 800-nM-aptamer/PAA/n-Pt sensors (Figure 13J). The LODs were 51.50 ±11.46 and 42.42 ± 12.36 CFU/mL and the sensitivity values were 1.81 ± 1.37 and 0.69 ± 1.42 (1/log(CFU/mL) using Z and R_{ct} data, respectively. Despite of some randomly trapping of bacteria on PAA brushes, these LOD and sensitivity results demonstrate the aptamers role of selectively binding to *L. monocytogenes* and significantly enhancing the performance of the sensors fabricated with PAA brushes.

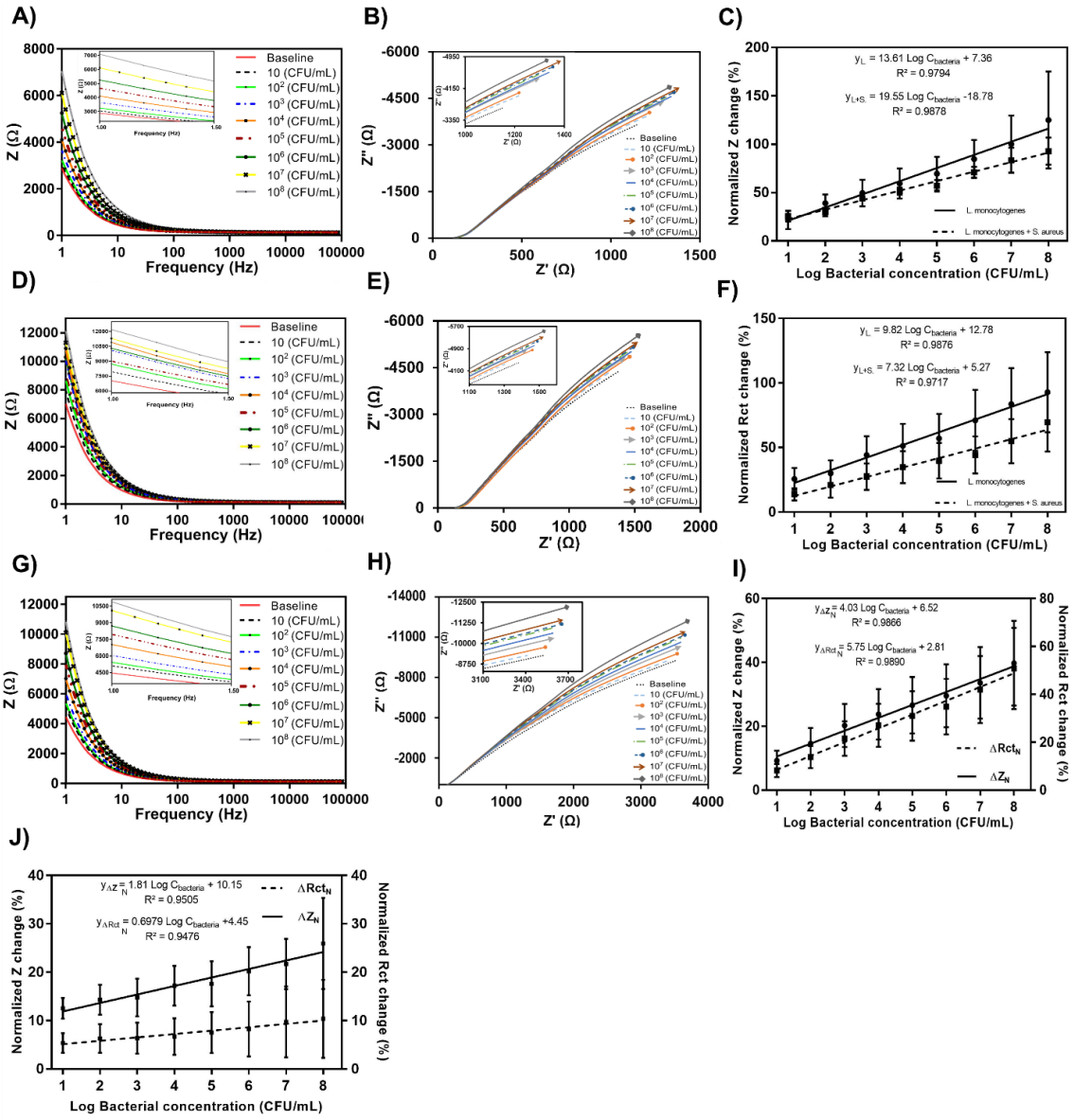

Figure 13: Detection of *L. monocytogene*s using 800-nM-aptamer/PAA/n-Pt biosensors. Bacteria concentration ranged from 10^1 to 10^8 CFU/mL. A), B), and G) are Bode plots obtained from the detection of *L. monocytogenes* in PBS, in PBS in the presence of *S. aureus* and in vegetable broth, respectively, the inset shows the impedance values at 1Hz. B), E), and H) are Nyquist plots obtained from the detection of *L. monocytogenes* in PBS, in PBS in the presence of *S. aureus* and in vegetable broth, respectively, the inset shows the impedance values at 1 Hz. C) and F) are calibration curves for detecting *L. monocytogenes* alone and *L. monocytogenes* with *S. aureus*, in PBS plotted using normalized impedance (Z) and normalized charge transfer resistance (R_{ct}) change, respectively. I) and J) are calibration curves for detecting *L. monocytogenes* in vegetable broth, and in the absence of aptamers in PBS, respectively, plotted using normalized Z change and normalized R_{ct} change. Error bars were based on the standard deviations (n ≥ 3). Normalized Z change and normalized R_{ct} change were calculated using Eq. 4.5 and 4.6, respectively.

Despite of some variation of the performance values using Z and R_{ct} changes, the developed biosensors, in this study, are superior to most biosensor performance parameters published for the detection of *L. monocytogenes*. The variation between the two approaches used to obtain the performance parameters can be linked to the method of analysis. R_{ct} values in this study were obtained using Zman software (WonATech Co.) that simulates the EIS data with the Randles equivalent circuit model and, takes into account the impedance readings across all the frequency spectrum, whereas, Z based results are obtained at 1 Hz only. In addition, one approach would at times provide more consistent results (i.e., higher R^2 (coefficient of determination) for calibration curves) than the other depending on the biosensor's platform One example would be for 800-nM-aptamer/PAA/n-Pt platform (Figure 13C and F) where Z change showed best results compared to R_{ct} change. Overall, R_{ct} data produced more consistent results taking into account all the impedance data over the frequency spectrum for this work.

Table 2 summarizes the performance parameters of biosensors developed in this work and the most recent reported sensors for the detection of *L. monocytogenes*. The study by Hills, (2016) reported a LOD of 9.1 ± 1.1 CFU/mL using aptasensor modified with chitosan, platinum and reduced graphene with a detection range of 10^1-10^7 CFU/mL in PBS. The LOD increased considerably to 31.12 ± 0.64 CFU/mL, when examining this biosensor in a real food sample (Hills, 2016).

Table 2: Comparison of biosensors performance parameters for detection of *Listeria monocytogenes.*

Biorecognition agent and Platform	Detection Mode	Test Medium	Sensitivity (1/log(CFU/mL))	Limit of Detection (CFU/mL)	Detection Range (CFU/mL)	Response time (min)	Reference
1000 nM aptamer + CHI + n-Pt	Impedimetric	PBS	R:14.57 ± 2.24[a] Z: 9.05 ± 1.55[a,b]	R: 3.75 ± 0.50[a,b] Z: 4.37 ± 0.86[a,b]	10^1-10^8	17	This work
400 nM aptamer + ALG + n-Pt	Impedimetric	PBS	R: 7.24 ± 1.91[b] Z: 27.98 ± 3.15[d]	R: 7.98 ± 1.72[a,b] Z: 1.17 ± 1.62[a]	10^1-10^8	17	This work
800 nM aptamer + PAA + n-Pt	Impedimetric	PBS	R: 9.82 ± 2.29[a,b] Z: 13.61 ± 2.73[a,b,c]	R: 5.46 ± 4.70[a,b] Z: 5.90 ± 4.21[a,b]	10^1-10^8	17	This work
1000 nM aptamer + CHI + n-Pt	Impedimetric	PBS + *S. aureus*	R:18.25 ± 3.00[a,c] Z: 10.64 ± 1.22[a,b]	R: 3.67 ± 3.34[a,b] Z: 6.10 ± 3.90[a,b]	10^1-10^8	17	This work
400 nM aptamer + ALG + n-Pt	Impedimetric	PBS + *S. aureus*	R: 6.05 ± 0.46[b,e] Z: 23.51 ± 3.00[c,d]	R: 10.2 ±1.13[a,b] Z: 4.76 ± 1.14[a,b]	10^1-10^8	17	This work
800 nM aptamer + PAA + n-Pt	Impedimetric	PBS + *S. aureus*	R: 7.32 ± 2.50[b] Z: 19.55 ± 3.47[a,c]	R: 4.45 ±3.90[a,b] Z: 3.72 ±3.02[a,b]	10^1-10^8	17	This work
1000 nM aptamer + CHI + n-Pt	Impedimetric	Vegetable Broth	R: 7.27 ± 1.10[b,e] Z: 4.74 ± 0.70[b,e]	R: 1.37 ± 1.50[a] Z: 3.36 ± 1.46[a,b]	10^1-10^8	17	This work
400 nM aptamer + ALG + n-Pt	Impedimetric	Vegetable Broth	R: 5.97 ± 0.90[b,e] Z: 22.83 ± 1.84[c,d]	R: 6.10 ± 1.95[a,b] Z: 6.95 ± 1.63[a,b]	10^1-10^8	17	This work
800 nM aptamer + PAA + n-Pt	Impedimetric	Vegetable Broth	R: 5.75 ± 1.85[b,e] Z: 4.03 ± 2.07[b,e]	R: 8.35 ± 6.22[a,b] Z: 11.35 ± 3.16[b]	10^1-10^8	17	This work
PGP + 100 nM amine aptamers	Impedimetric	PBS	2.27 ± 0.28	47.4.4 ± 3.36	10^2-10^8	17	(Hills, 2016)

Table 2: Continued

Biorecognition agent and Platform	Detection Mode	Test Medium	Sensitivity (1/log(CFU/mL))	Limit of Detection (CFU/mL)	Detection Range (CFU/mL)	Response time (min)	Reference
PGP + CHI + 100 nM aptamer	Impedimetric	PBS + *S. aureus*	14.25 ± 1.69	9.1 ± 1.1	10^1-10^7	17	(Hills, 2016)
PGP + CHI + 100 nM aptamers	Impedimetric	Vegetable Broth	3.76 ± 0.34	31.12 ± 0.64	10^2-10^8	17	(Hills, 2016)
PGP + 400 nM thiol aptamers	Impedimetric	PBS	9.81 ± 2.0	11.2 ± 0.79	10^2-10^8	17	(Hills, 2016)
PGP + CHI + 100 nM aptamers	Impedimetric	PBS	12.14 ± 1.79	9.1 ± 1.1	10^1-10^8	17	(Hills, 2016)
PGP + 50 nM antibodies	Impedimetric	PBS	1.13 ± 0.175	85.9 ± 3.73	10^2-10^8	17	(Hills, 2016)
PGP + CHI + 200 nM antibodies	Impedimetric	Vegetable Broth	4.9 ± 0.4	23.9 ± 0.96	10^2-10^7	17	(Hills, 2016)
Pt-IMEs + aptamer	Impedimetric	Vegetable Broth	268.1 ± 25.40 (Ohms/log (CFU/mL))	4.82 ± 0.01	10^1-10^7	12	(Sidhu, 2015)
Pt-IMEs + aptamer	Impedimetric	PBS	268.1 ± 25.40 (Ohms/log (CFU/mL))	5.39 ± 0.21	10^1-10^6	17	(Sidhu et al., 2016)
AuNPS + SPCE + Antibodies	Amperometric	Stomached blueberry	Not reported	10^2	10^2-10^5	60	(Davis et al., 2013)
GNP + Antibodies	Dynamic Light Scattering	PBS	Not reported	35	3.5 x 10^1-10^3	120	(Huang et al., 2015)

Table 2: Continued

Biorecognition agent and Platform	Detection Mode	Test Medium	Sensitivity (1/log(CFU/mL))	Limit of Detection (CFU/mL)	Detection Range (CFU/mL)	Response time (min)	Reference
GNP + Antibodies	Dynamic Light Scattering	Lettuce homogenized in water	Not reported	22	3.5×10^{1}-10^{3}	180	(Huang et al., 2015)
Aptamer + Fe_3O_4 NPC	Colorimetric	Milk	Not reported	5.4×10^{3}	5.4×10^{3}-10^{8}	145	(Zhang et al., 2016)
None	Real-Time PCR	Sausage and ham homogenized in Fraser broth	Not reported	$1 - 10^{2}$ depending upon the sample	Not reported	540-600	(Heo et al., 2014)

Values given are averages of 3 replicates ± standard deviations. Average values with different superscript letters (within columns) indicate significant differences ($p < 0.05$).
R: values based on R_{ct} percentage change data
Z: values based on total impedance (Z) percentage change data
AuNPS and GNP: Gold nanoparticles
SPCE: Screen-printed carbon electrode
NPC: Nanoparticles cluster

Other biosensors that used antibodies as biorecognition agent reported a minimum LOD of 22 CFU/mL (Davis et al., 2013; Hills, 2016; Huang et al., 2015). Zhang et al (2016) developed a colorimetric assay functionalized with aptamer and nanoparticle cluster for *L. monocytogenes* visual detection. The designed biosensors yielded LOD of 5.4×10^3 CFU/mL and a detection range of 5.4×10^3-10^8 CFU/mL in 145 min (Zhang et al., 2016). Not only the LOD but also the response time of this biosensor were significantly higher to achieve the reported detection results compared to the current work. Sidhu (2015) developed interdigitated microelectrodes array using the same aptamer of this work, as a biorecognition element, for the detection of *L. monocytogenes* and reported 4.82 ± 0.01 CFU/mL LOD, 10^1-10^7 CFU/mL detection range, and 12 min response time when sensing in vegetable broth. Only the study by Sidhu (2015) reported shorter response time than this study, 12 min compared to 17 min. Other studies reported considerably longer time (Davis et al., 2013; Heo et al., 2014; Huang et al., 2015; Zhang et al., 2016).

Lower LOD was achieved in this work using 1000-nM-aptamer/CHI/n-Pt biosensor based on R_{ct} data in a similar media (1.37 ± 1.50 CFU/mL). In addition, 1000-nM-aptamer/CHI/n-Pt biosensor, in this study, had the lowest average LOD in vegetable broth (1.37 ± 1.50 CFU/mL R_{ct} based and 3.36 ± 1.46 CFU/mL Z based) compared to 400-nM-aptamer/ALG/n-Pt biosensor (6.10 ± 1.95 CFU/mL R_{ct} based and 6.95 ± 1.63 CFU/mL Z based) and 800-nM-aptamer/PAA/n-Pt biosensor (8.35 ± 6.22 CFU/mL R_{ct} based and 11.35 ±

3.16CFU/mL Z based). The lowest average LOD obtained in PBS was with 400-nM-aptamer/ALG/n-Pt biosensors, which also had the highest sensitivity average in this study based on Z values (1.17 ± 1.62 CFU/mL and 27.98 ± 3.15 (1/log(CFU/mL)), respectively).

Moreover, 800-nM-aptamer/PAA/n-Pt biosensors had the highest average LODs in complex sample (8.35 ± 6.22 CFU/mL R_{ct} based and 11.35 ± 3.16 CFU/mL Z based) with the lowest average sensitivity among the test platforms (5.75 ± 1.85 and 4.03 ± 2.07(1/log(CFU/mL)) based on R_{ct} and Z, respectively). Despite of these parameters, 800-nM-aptamer/PAA/n-Pt biosensors outweigh most of the published biosensors for *L. monocytogenes* detection. Although 1000-nM-aptamer/CHI/n-Pt biosensor had the overall leading performance parameters, the high attachment of *L. monocytogenes* on the CHI brushes when testing without aptamers makes the 400-nM-aptamer/ALG/n-Pt biosensor the best platform developed in this study with LOD of (6.10 ± 1.95 CFU/mL and 6.95 ± 1.63 CFU/mL based on R_{ct} and Z, respectively) and sensitivity of (5.97 ± 0.90 and 22.83 ± 1.84 (1/log(CFU/mL)) based on R_{ct} and Z, respectively) in complex media

CHAPTER V

CONCLUSIONS

In this study, three different biosensor's platforms were designed and tested for the detection of *Listeria monocytogenes* using aptamers as biorecognition agents. The bare electrodes were initially coated with nanoplatinum (n-Pt) for 140 sec using pulSED methodincreasing significantly the ESA from 0.018 ± 0.0004 cm^2 to 0.081 ± 0.0179 cm^2 for bare and n-Pt electrodes, respectively. The n-Pt electrodes were then electrodeposited and optimized with pH-responsive polymers, CHI, ALG and PAA, to create stimuli-responsive nanobrushes, which showed to enhance the sensors performance by increasing ($P < 0.05$) the ESA and the interaction between the biorecognition agents and the tested medium and consequently, the target bacteria as well as improving the sensing procedure. The ESA for optimized CHI, ALG, and PAA/n-Pt modified electrodes were 0.101 ± 0.004 cm^2, 0.111 ± 0.012 cm^2, and 0.108 ± 0.022 cm^2; respectively; and the optimum aptamer loading concentrations were 1000 nM for CHI/n-Pt, 400 nM for ALG/n-Pt, and 800 nM for PAA/n-Pt electrodes. Actuation tests demonstrated the extension and contraction of the polymer brushes based on pH changes and the best pH conditions for testing were identified. Aptamer/CHI/n-Pt electrodes were found to best capture bacteria at pH 4 and to sense at pH 8, while aptamer/ALG/n-Pt and aptamer/PAA/n-Pt performed the best at pH 7.5 and pH 3.5 for capturing and sensing, respectively; this confirming the basic concept of brush actuation and

proved that nanobrush actuation in stagnant media improves cell capture (relative to no actuation). The developed biosensors were tested in three different media and had a rapid detection time of 17 min and a wide detection range of 10^1-10^8 CFU/mL of *L. monocytogenes*. The designed biosensors had no significant difference ($p > 0.05$) in LODs when testing in PBS and in vegetable when comparing each platform individually, demonstrating the selectivity of the biosensors. Overall, the 1000-nM-aptamer/CHI/n-Pt biosensors provided the lowest average of limits of detection (LODs), 1.37 ± 1.50 and 3.36 ± 1.46 CFU/mL with a sensitivity of 7.27 ± 1.10 and 4.74 ± 0.70 (1/log(CFU/mL)) based on R_{ct} and Z data, respectively. Conversely, the 400-nM-aptamer/ALG/n-Pt biosensors provided the most consistent results with LODs of 6.10 ± 1.95 and 6.95 ± 1.63 CFU/mL and sensitivity of 5.97 ± 0.90 and 22.83 ± 1.84 (1/log(CFU/mL)) based on R_{ct} and Z data, respectively.

Incorporation of aptamers, pH-responsive polymers and nanoplatinum resulted in highly sensitive, selective, rapid and label-free electrochemical biosensors that can be used for real-time detection of *L. monocytogenes*. These biosensors can easily be modified to detect other pathogens and could be used in future foodborne detection replacing traditional methods. Furthermore, the designed biosensors could be further developed to become portable making the steps for ensuring public health more accessible.

CHAPTER VI

FUTURE RECOMMENDATIONS

Based on the findings in this study further improvement on electrochemical impedance aptasensors for the detection of *L. monocytogenes* could be achieved by addressing the following:

- Determine the best approach for characterizing the biosensors electrochemically, by evaluating different frequencies, total impedance, imaginary and real impedance, charge transfer resistance, and other components on Randles equivalent circuit.
- Study the shelf life of the biosensors and finding the optimum storage conditions for best biosensor performance and cost efficiency.
- Test the reusability by examining different washing techniques considering the aptamers reloading and its impact on the performance.
- Attach polymer brushes using pulsed sonoelectrodeposition (pulSED) technique and comparing the structure obtained with this electrodeposition method.
- Replace the Pt/Ir base electrodes with paper based electrodes or other inexpensive environmentally-friendly electrodes to reduce the overall costs.
- Determine biosensor performance using different food samples and different interferences to confirm biosensor performance and design sample preparation methods for regular food products.

- Test the biosensors performance in the present of non-viable cells to understand the effect caused on sensor performance.
- Explore different aptamers with higher binding affinities that are selective toward *L. monocytogenes* using different loading approaches (i.e., entrapment or different bioconjugation cross linking methods).
- Explore different biorecognition agents including antibodies and aptamers.
- Improve the software currently used to become user-friendly and minimize the system setup to become portable and accessible for use in varying environments.
- Test different pH-responsive polymers such as polylactic acid as well as other stimuli responsive polymers including temperature and electrical responsive polymers.
- Deposit n-Pt using pulSED technique with different voltages and characterize the particle size formed and ESA achieved.

REFERENCES

Allerberger, F., & Wagner, M. (2010). Listeriosis : a resurgent foodborne infection. *Clinical Microbiology and Infection*, *16*(1), 16–23.

Axelrod, T., Eltzov, E., & Marks, R. S. (2016). Bioluminescent bioreporter pad biosensor for monitoring water toxicity. *Talanta*, *149*, 290–297. https://doi.org/10.1016/j.talanta.2015.11.067

Badhulika, S., Paul, R. K., Rajesh, T., Terse, T., & Mulchandani, A. (2014). Nonenzymatic glucose sensor based on platinum nanoflowers decorated multiwalled carbon nanotubes-graphene hybrid electrode. *Electroanalysis*, *26*(1), 103–108. https://doi.org/10.1002/elan.201300286

Balamurugan, S., Obubuafo, A., Soper, S. A., & Spivak, D. A. (2008). Surface immobilization methods for aptamer diagnostic applications. *Analytical and Bioanalytical Chemistry*, *390*(4), 1009–1021. https://doi.org/10.1007/s00216-007-1587-2

Belgacem, M., & Gandini, A. (2008). *Monomers, polymers and composites from renewable resources* (1st ed). Boston,: MA: Elsevier.

Bhakta, S. A., Benavidez, T. E., & Garcia, C. D. (2014). Immobilization of glucose oxidase to nanostructured films of polystyrene-block-poly(2-vinylpyridine). *Journal of Colloid and Interface Science*, *430*, 351–356. https://doi.org/10.1016/j.jcis.2014.05.067

Bruno, J. G., Phillips, T., Montez, T., Garcia, A., Sivils, J. C., Mayo, M. W., & Greis, A. (2015). Development of a fluorescent enzyme-linked DNA aptamer-magnetic bead sandwich assay and portable fluorometer for sensitive and rapid listeria Detection. *Journal of Fluorescence*, *25*(1), 173–183. https://doi.org/10.1007/s10895-014-1495-8

Burrs, S. L., Bhargava, M., Sidhu, R., Kiernan-Lewis, J., Gomes, C., Claussen, J. C., & McLamore, E. S. (2016). A paper based graphene-nanocauliflower hybrid composite for point of care biosensing. *Biosensors and Bioelectronics*, *85*, 479–487. https://doi.org/10.1016/j.bios.2016.05.037

Burrs, S. L., Vanegas, D. C., Bhargava, M., Mechulan, N., Hendershot, P., Yamaguchi, H., & McLamore, E. S. (2015). A comparative study of graphene-hydrogel hybrid bionanocomposites for biosensing. *The Analyst*, *140*(5), 1466–76. https://doi.org/10.1039/c4an01788a

CDC. (2016a). Foodborne germs and illnesses. Retrieved June 6, 2016, from https://www.cdc.gov/foodsafety/foodborne-germs.html

CDC. (2016b). Foodborne outbreak online database (FOOD Tool). Retrieved April 6, 2017, from https://wwwn.cdc.gov/foodborneoutbreaks/

CDC. (2016c). *Listeria* outbreaks | *listeria* | CDC. Retrieved August 17, 2016, from http://www.cdc.gov/listeria/outbreaks/index.html

Chaturvedi, P., Vanegas, D. C., Taguchi, M., Burrs, S. L., Sharma, P., & McLamore, E. S. (2014). A nanoceria-platinum-graphene nanocomposite for electrochemical biosensing. *Biosensors and Bioelectronics*, *58*, 179–185. https://doi.org/10.1016/j.bios.2014.02.021

Cheong, M., & Zhitomirsky, I. (2008). Electrodeposition of alginic acid and composite films. *Colloids and surfaces a: physicochemical and engineering aspects*, *328*(1–3), 73–78. https://doi.org/10.1016/j.colsurfa.2008.06.019

Chetia, T. R., Ansari, M. S., & Qureshi, M. (2016). Rational design of hierarchical ZnO superstructures for efficient charge transfer: mechanistic and photovoltaic studies of hollow, mesoporous, cage-like nanostructures with compacted 1D building blocks. *Phys. Chem. Chem. Phys.*, *18*(7), 5344–5357. https://doi.org/10.1039/C5CP07687K

Cook, J. P., & Riley, D. J. (2012). pH induced swelling of PVP microgel particles - A first order phase transition? *Journal of Colloid and Interface Science*, *370*(1), 67–72. https://doi.org/10.1016/j.jcis.2011.12.064

Crivianu-Gaita, V., & Thompson, M. (2016). Aptamers, antibody scFv, and antibody Fab' fragments: An overview and comparison of three of the most versatile biosensor biorecognition elements. *Biosensors and Bioelectronics*, *85*, 32–45. https://doi.org/10.1016/j.bios.2016.04.091

Cui, L., Jia, J., Guo, Y., Liu, Y., & Zhu, P. (2014). Preparation and characterization of IPN hydrogels composed of chitosan and gelatin cross-linked by genipin. *Carbohydrate Polymers*, *99*, 31–38. https://doi.org/10.1016/j.carbpol.2013.08.048

Davis, D., Guo, X., Musavi, L., Lin, C.-S., Chen, S.-H., & Wu, V. C. H. (2013). Gold nanoparticle-modified carbon electrode biosensor for the detection of *Listeria monocytogenes*. *Industrial Biotechnology*, *9*(1), 31–36. https://doi.org/10.1089/ind.2012.0033

De Giglio, E., Cometa, S., Cioffi, N., Torsi, L., & Sabbatini, L. (2007). Analytical investigations of poly(acrylic acid) coatings electrodeposited on titanium-based implants: A versatile approach to biocompatibility enhancement. *Analytical and Bioanalytical Chemistry*, *389*(7–8), 2055–2063. https://doi.org/10.1007/s00216-007-1299-7

Diaconu, M., Litescu, S. C., & Radu, G. L. (2010). Laccase-MWCNT-chitosan biosensor-A new tool for total polyphenolic content evaluation from in vitro cultivated plants. *Sensors and Actuators, B: Chemical*, *145*(2), 800–806. https://doi.org/10.1016/j.snb.2010.01.064

Duan, N., Ding, X., He, L., Wu, S., Wei, Y., & Wang, Z. (2013). Selection , identi fi cation and application of a DNA aptamer against *Listeria monocytogenes*. *Food Control*, *33*(1), 239–243. https://doi.org/10.1016/j.foodcont.2013.03.011

Elliott, J. E., MacDonald, M., Nie, J., & Bowman, C. N. (2004). Structure and swelling of poly(acrylic acid) hydrogels: Effect of pH, ionic strength, and dilution on the crosslinked polymer structure. *Polymer*, *45*(5), 1503–1510. https://doi.org/10.1016/j.polymer.2003.12.040

Erdem, A., Eksin, E., & Muti, M. (2014). Chitosan-graphene oxide based aptasensor for the impedimetric detection of lysozyme. *Colloids and Surfaces B: Biointerfaces*, *115*, 205–211. https://doi.org/10.1016/j.colsurfb.2013.11.037

Galaev, I., & Mattiasson, B. (2001). *Smart polymers for bioseparation and bioprocessing*. CRC Pres. https://doi.org/9781439858165

Grieshaber, D., Mackenzie, R., Vörös, J., & Reimhult, E. (2008). Electrochemical biosensors -sensor principles and architectures. *Sensors*, *8*(March), 1400–1458. https://doi.org/10.3390/s8031400

Heo, E. J., Song, B. R., Park, H. J., Kim, Y. J., Moon, J. S., Wee, S. H., & Yoon, Y. (2014). Rapid detection of *Listeria monocytogenes* by real-time PCR in processed meat and dairy products. *Journal of Food Protection*, *77*(3), 453–458. https://doi.org/10.4315/0362-028X.JFP-13-318

Hida, T. (1980). Brownian motion. In *Brownian motion* (pp. 44–113). New York, NY: Springer US. https://doi.org/10.1007/978-1-4612-6030-1_2

Hills, K. D. (2016). *Aptasensor based approach for real-time monitoring of listeria innocua and Listeria monocytogenes*. Texas A & M University. Retrieved from http://hdl.handle.net/1969.1/156824

Huang, J., Yang, G., Meng, W., Wu, L., Zhu, A., & Jiao, X. (2010). An electrochemical impedimetric immunosensor for label-free detection of Campylobacter jejuni in diarrhea patients' stool based on O-carboxymethylchitosan surface modified Fe3O4 nanoparticles. *Biosensors and Bioelectronics*, *25*(5), 1204–1211. https://doi.org/10.1016/j.bios.2009.10.036

Huang, X., Xu, Z., Mao, Y., Ji, Y., Xu, H., Xiong, Y., & Li, Y. (2015). Gold nanoparticle-based dynamic light scattering immunoassay for ultrasensitive detection of *Listeria monocytogenes* in lettuces. *Biosensors and Bioelectronics*, *66*(November), 184–190. https://doi.org/10.1016/j.bios.2014.11.016

Hunter, G. W., Mukundan, R., & Bhansali, S. (2008). *Sensors, actuators, and microsystems (general), Issue 20*. Electrochemical Society.

Jabbari, E., & Nozari, S. (2000). Swelling behavior of acrylic acid hydrogels prepared by ??-radiation crosslinking of polyacrylic acid in aqueous solution. *European Polymer Journal*, *36*(12), 2685–2692. https://doi.org/10.1016/S0014-3057(00)00044-6

Jantra, J., Kanatharana, P., Asawatreratanakul, P., Hedström, M., Mattiasson, B., & Thavarungkul, P. (2011). Real-time label-free affinity biosensors for enumeration of total bacteria based on immobilized concanavalin A. *Journal of Environmental Science and Health. Part A, Toxic/hazardous Substances & Environmental Engineering*, *46*(13), 1450–60. https://doi.org/10.1080/10934529.2011.609022

Jay, J., Loessner, M., & Golden, D. (2008). *Modern food microbiology*. Springer Science & Business Media.

Ju, H. K., Kim, S. Y., & Lee, Y. M. (2001). pH/temperature-responsive behaviors of semi-IPN and comb-type graft hydrogels composed of alginate and poly(N-isopropylacrylamide). *Polymer*, *42*(16), 6851–6857. https://doi.org/10.1016/S0032-3861(01)00143-4

Khiar, A. S. A., Puteh, R., & Arof, A. K. (2006). Conductivity studies of a chitosan-based polymer electrolyte. *Physica B: Condensed Matter*, *373*(1), 23–27. https://doi.org/10.1016/j.physb.2005.10.104

Kissinger, P. T., & Heineman, W. R. (1983). Cyclic voltammetry. *Journal of Chemical Education*, *60*(9), 9242–5. https://doi.org/10.1002/anie.201004874

Kong, F.-Y., Gu, S.-X., Li, W.-W., Chen, T.-T., Xu, Q., & Wang, W. (2014). A paper disk equipped with graphene/polyaniline/Au nanoparticles/glucose oxidase biocomposite modified screen-printed electrode: Toward whole blood glucose determination. *Biosensors and Bioelectronics*, *56*, 77–82. https://doi.org/10.1016/j.bios.2013.12.067

Krishnamoorthy, M., Hakobyan, S., Ramstedt, M., & Gautrot, J. E. (2014). Surface-initiated polymer brushes in the biomedical field: Applications in membrane science, biosensing, cell culture, regenerative medicine and antibacterial coatings. *Chemical Reviews*, *114*(21), 10976–11026. https://doi.org/10.1021/cr500252u

Kurniawan, F., Tsakova, V., & Mirsky, V. M. (2006). Gold nanoparticles in nonenzymatic electrochemical detection of sugars. *Electroanalysis*, *18*(19–20), 1937–1942. https://doi.org/10.1002/elan.200603607

Lazcka, O., Campo, F. J. Del, & Muñoz, F. (2007). Pathogen detection: A perspective of traditional methods and biosensors. *Biosensors and Bioelectronics*, *22*(7), 1205–1217. https://doi.org/10.1016/j.bios.2006.06.036

Lee, S., Ahn, J., Lee, K., Um, H., Singh, S., Sun, T., & Kim, Y. (2015). Analytical bioconjugates, aptamers, enable specific quantitative detection of *Listeria monocytogenes*, *68*, 272–280.

Lee, T., & Niederer, P. (2010). *Basic engineering for medics and biologists: An ESEM primer*. Washington, DC: IOS Press.

Lin, H., Lu, Q., Ge, S., Cai, Q., & Grimes, C. A. (2010). Detection of pathogen *Escherichia coli O157:H7* with a wireless magnetoelastic-sensing device amplified by using chitosan-modified magnetic Fe3O4 nanoparticles. *Sensors and Actuators, B: Chemical*, *147*(1), 343–349. https://doi.org/10.1016/j.snb.2010.03.011

Liu, C., Guo, X., Cui, H., & Yuan, R. (2009). An amperometric biosensor fabricated from electro-co-deposition of sodium alginate and horseradish peroxidase. *Journal of Molecular Catalysis B: Enzymatic*, *60*(3–4), 151–156. https://doi.org/10.1016/j.molcatb.2009.04.015

López-León, T., Carvalho, E. L. S., Seijo, B., Ortega-Vinuesa, J. L., & Bastos-González, D. (2005). Physicochemical characterization of chitosan nanoparticles: Electrokinetic and stability behavior. *Journal of Colloid and Interface Science*, *283*(2), 344–351. https://doi.org/10.1016/j.jcis.2004.08.186

Luo, P., Liu, Y., Xia, Y., Xu, H., & Xie, G. (2014). Aptamer biosensor for sensitive detection of toxin A of Clostridium difficile using gold nanoparticles synthesized by Bacillus stearothermophilus. *Biosensors and Bioelectronics*, *54*(April), 217–221. https://doi.org/10.1016/j.bios.2013.11.013

Luo, X.-L., Xu, J.-J., Du, Y., & Chen, H.-Y. (2004). A glucose biosensor based on chitosan–glucose oxidase–gold nanoparticles biocomposite formed by one-step electrodeposition. *Analytical Biochemistry*, *334*(2), 284–289. https://doi.org/10.1016/j.ab.2004.07.005

Lvovich, V. F. (2012). *Impedance spectroscopy : applications to electrochemical and dielectric phenomena*. New Jersy: John Wiley & Sons.

Ma, Q., Sun, H., & Hou, S. (2013). Application of graphene oxide sheets incorporated in the porous calcium alginate films on the glassy carbon electrode for biosensor construction based on myoglobin. *Journal of Applied Electrochemistry*, *43*(10), 975–984. https://doi.org/10.1007/s10800-013-0595-5

Maalouf, R., Hassen, W. M., Fournier-Wirth, C., Coste, J., & Jaffrezic-Renault, N. (2008). Comparison of two innovatives approaches for bacterial detection: Paramagnetic nanoparticles and self-assembled multilayer processes. In *Microchimica Acta* (Vol. 163, pp. 157–161). https://doi.org/10.1007/s00604-008-0008-3

Mallikarjuna Reddy, K., Ramesh Babu, V., Krishna Rao, K. S. V, Subha, M. C. S., Chowdoji Rao, K., Sairam, M., & Aminabhavi, T. M. (2007). Temperature sensitive semi-ipn microspheres from sodium alginate and n-isopropylacrylamide for controlled release of 5-fluorouracil. *Journal of Applied Polymer Science*, *107*(5), 2820–2829.

Maturin, L., & Peeler, J. (2015). Laboratory methods - bam: aerobic plate count. Retrieved from http://www.fda.gov/Food/FoodScienceResearch/LaboratoryMethods/ucm063346.htm

Medina, R. P. . B., Nadres, E. T. ., Ballesteros F.C., J. ., & Rodrigues, D. F. . (2016). Incorporation of graphene oxide into a chitosan-poly(acrylic acid) porous polymer nanocomposite for enhanced lead adsorption. *Environmental Science: Nano*, *3*(3), 638–646. https://doi.org/10.1039/c6en00021e

Melo, J., Andrew, P. W., & Faleiro, M. L. (2015). *Listeria monocytogenes* in cheese and the dairy environment remains a food safety challenge: The role of stress responses. *Food Research International*. Elsevier Ltd. https://doi.org/10.1016/j.foodres.2014.10.031

Ohk, S. H., Koo, O. K., Sen, T., Yamamoto, C. M., & Bhunia, A. K. (2010). Antibody-aptamer functionalized fibre-optic biosensor for specific detection of *Listeria monocytogenes* from food. *Journal of Applied Microbiology*, *109*(3), 808–817. https://doi.org/10.1111/j.1365-2672.2010.04709.x

Ozawa, F., Ino, K., Takahashi, Y., Shiku, H., & Matsue, T. (2013). Electrodeposition of alginate gels for construction of vascular-like structures. *Journal of Bioscience and Bioengineering*, *115*(4), 459–461. https://doi.org/10.1016/j.jbiosc.2012.10.014

Parkash, M., & Skladal, P. (2008). Electrochemical biosensors, principles and aplications. *Journal Of Applied Biomedicine*, (January), 57–64.

Pasparakis, G., & Bouropoulos, N. (2006). Swelling studies and in vitro release of verapamil from calcium alginate and calcium alginate-chitosan beads. *International Journal of Pharmaceutics*, *323*(1–2), 34–42. https://doi.org/10.1016/j.ijpharm.2006.05.054

Pradeep, T. (2012). *A textbook of nanoscience and nanotechnology*. New Delhi: Tata McGraw Hill Education. Retrieved from http://www.worldcat.org/title/textbook-of-nanoscience-and-nanotechnology/oclc/831264199

Prodromidis, M. I. (2010). Impedimetric immunosensors-A review. *Electrochimica Acta*, *55*(14), 4227–4233. https://doi.org/10.1016/j.electacta.2009.01.081

Radhakrishnan, R., Jahne, M., Rogers, S., & Suni, I. I. (2013). Detection of *Listeria monocytogenes* by electrochemical impedance spectroscopy. *Electroanalysis*, *25*(9), 2231–2237. https://doi.org/10.1002/elan.201300140

Radi, A.-E. (2011). Electrochemical aptamer-based biosensors: recent advances and perspectives. *International journal of electrochemistry*, *2011*, 1–17. https://doi.org/10.4061/2011/863196

Saha, K., Agasti, S. S., Kim, C., Li, X., & Rotello, V. M. (2012). Gold nanoparticles in chemical and biological sensing. *Chemical Reviews*, *112*(5), 2739–2779. https://doi.org/10.1021/cr2001178

Sanvicens, N., Pastells, C., Pascual, N., & Marco, M.-P. (2009). Nanoparticle-based biosensors for detection of pathogenic bacteria. *TrAC Trends in Analytical Chemistry*, *28*(11), 1243–1252. https://doi.org/10.1016/j.trac.2009.08.002

Sapsford, K. E., Tyner, K. M., Dair, B. J., Deschamps, J. R., & Medintz, I. L. (2011). Analyzing nanomaterial bioconjugates: a review of current and emerging purification and characterization techniques. *Analytical Chemistry*, *83*(12), 4453–4488. https://doi.org/10.1021/ac200853a

Sarwate, V. V. (1993). *Electromagnetic fields and waves*. Wiley.

Scallan, E., Hoekstra, R. M., Angulo, F. J., Tauxe, R. V., Widdowson, M. A., Roy, S. L., & Griffin, P. M. (2011). Foodborne illness acquired in the united states-major pathogens. *Emerging Infectious Diseases*, *17*(1), 7–15. https://doi.org/10.3201/eid1701.P11101

Scharff, R. L. (2012). Economic burden from health losses due to foodborne illness in the united states. *Journal of Food Protection*, *75*(1), 123–131. https://doi.org/10.4315/0362-028X.JFP-11-058

Sharma, H., & Mutharasan, R. (2013). Review of biosensors for foodborne pathogens and toxins. *Sensors and Actuators, B: Chemical*, *183*, 535–549. https://doi.org/10.1016/j.snb.2013.03.137

Sharma, R., Ragavan, K. V., Thakur, M. S., & Raghavarao, K. S. M. S. (2015). Recent advances in nanoparticle based aptasensors for food contaminants. *Biosensors and Bioelectronics*. https://doi.org/10.1016/j.bios.2015.07.017

Shi, X., Zheng, Y., Wang, G., Lin, Q., & Fan, J. (2014). pH- and electro-response characteristics of bacterial cellulose nanofiber/sodium alginate hybrid hydrogels for dual controlled drug delivery. *RSC Adv.*, *4*(87), 47056–47065. https://doi.org/10.1039/C4RA09640A

Sidhu, R. (2015). *Aptamer Based Lab-On-A-Chip Biosensor For Selective Detection Of Foodborne Pathogen, Listeria Spp., In Food Products*. Texas A&M University.

Sidhu, R., Rong, Y., Vanegas, D. C., Claussen, J., McLamore, E. S., & Gomes, C. (2016). Impedance biosensor for the rapid detection of Listeria spp. based on aptamer functionalized Pt-interdigitated microelectrodes array, *9863*, 98630F. https://doi.org/10.1117/12.2223443

Singh, A., Sinsinbar, G., Choudhary, M., Kumar, V., Pasricha, R., Verma, H. N., & Arora, K. (2013). Graphene oxide-chitosan nanocomposite based electrochemical DNA biosensor for detection of typhoid. *Sensors and Actuators, B: Chemical*, *185*(August 2013), 675–684. https://doi.org/10.1016/j.snb.2013.05.014

Sozer, N., & Kokini, J. L. (2009). Nanotechnology and its applications in the food sector. *Trends in Biotechnology*, *27*(2), 82–9. https://doi.org/10.1016/j.tibtech.2008.10.010

Stamenkovic, J., Premovic, P., & Mentus, S. (1997). Electrical conductivity of poly(acrylic acid) gels. *Journal of the Serbian Chemical Society*, 945–950. Retrieved from http://tesla.pmf.ni.ac.rs/lgc/articles/53-1997.pdf

Suh, S. H., Dwivedi, H. P., Choi, S. J., & Jaykus, L. A. (2014). Selection and characterization of DNA aptamers specific for Listeria species. *Analytical Biochemistry*, *459*(AUGUST), 39–45. https://doi.org/10.1016/j.ab.2014.05.006

Suh, S. H., & Jaykus, L.-A. (2013). Nucleic acid aptamers for capture and detection of Listeria spp. *Journal of Biotechnology*, *167*(4), 454–61. https://doi.org/10.1016/j.jbiotec.2013.07.027

Syed, L. U., Liu, J., Price, A. K., Li, Y. F., Culbertson, C. T., & Li, J. (2011). Dielectrophoretic capture of E. coli cells at micropatterned nanoelectrode arrays. *Electrophoresis*, *32*(17), 2358–2365. https://doi.org/10.1002/elps.201100020

Taguchi, M., Schwalb, N., Rong, Y., Vanegas, D. C., Garland, N., Tan, M., & McLamore, E. S. (2016). pulSED: pulsed sonoelectrodeposition of fractal nanoplatinum for enhancing amperometric biosensor performance. *The Analyst*, *141*(11), 3367–78. https://doi.org/10.1039/c6an00069j

Tan, F., Leung, P. H. M., Liu, Z. Bin, Zhang, Y., Xiao, L., Ye, W., & Yang, M. (2011). A PDMS microfluidic impedance immunosensor for E. coli O157:H7 and Staphylococcus aureus detection via antibody-immobilized nanoporous membrane. *Sensors and Actuators, B: Chemical*, *159*(1), 328–335. https://doi.org/10.1016/j.snb.2011.06.074

Terao, K. (2014). Poly(acrylic acid) (PAA). In S. Kobayashi & K. Müllen (Eds.), *Encyclopedia of polymeric nanomaterials* (pp. 1–6). Berlin, Heidelberg: Springer Berlin Heidelberg. https://doi.org/10.1007/978-3-642-36199-9_279-

Tokareva, I., Minko, S., Fendler, J., & Hutter, E. (2004). Polymer Brushes and Gold Nanoparticle Enhanced Transmission Surface Plasmon. *Journal Of The American Chemical Society*, *0*, 15950–15951. https://doi.org/10.1021/ja044575y

Vanegas, D. C., Rong, Y., Schwalb, N., Hills, K. D., Gomes, C., & McLamore, E. S. (2015). Rapid detection of listeria spp. using an internalin A aptasensor based on carbon-metal nanohybrid structures. *In SPIE Sensing Technology Applications* (pp. 948708-948708). International Society for Optics and Photonics. https://doi.org/10.1117/12.2177441

Vanegas, D. C., Taguchi, M., Chaturvedi, P., Burrs, S., Tan, M., Yamaguchi, H., & McLamore, E. S. (2014). A comparative study of carbon-platinum hybrid nanostructure architecture for amperometric biosensing. *The Analyst*, *139*(3), 660–7. https://doi.org/10.1039/c3an01718d

Varshney, M., & Li, Y. (2007). Interdigitated array microelectrode based impedance biosensor coupled with magnetic nanoparticle-antibody conjugates for detection of *Escherichia coli O157:H7* in food samples. *Biosensors and Bioelectronics*, *22*(11), 2408–2414. https://doi.org/10.1016/j.bios.2006.08.030

Vidal, J. C., Bonel, L., Ezquerra, A., Hernández, S., Bertolín, J. R., Cubel, C., & Castillo, J. R. (2013). Electrochemical affinity biosensors for detection of mycotoxins: A review. *Biosensors and Bioelectronics*, *49*, 146–158. https://doi.org/10.1016/j.bios.2013.05.008

Walderhaug, M. (2014). *Bad Bug Book: Foodborne pathogenic microorganisms and natural toxins handbook*. BrainFeed Press.

Wan, W., Dai, G., Zhang, L., & Shen, Y. (2015). Paper-based electrodeposition chip for 3D alginate hydrogel formation. *Micromachines*, *6*(10), 1546–1559. https://doi.org/10.3390/mi6101438

Wan, Y., Lin, Z., Zhang, D., Wang, Y., & Hou, B. (2011). Impedimetric immunosensor doped with reduced graphene sheets fabricated by controllable electrodeposition for the non-labelled detection of bacteria. *Biosensors and Bioelectronics*, *26*(5), 1959–1964. https://doi.org/10.1016/j.bios.2010.08.008

Wan, Y., Zhang, D., Wang, Y., & Hou, B. (2010). A 3D-impedimetric immunosensor based on foam Ni for detection of sulfate-reducing bacteria. *Electrochemistry Communications*, *12*(2), 288–291. https://doi.org/10.1016/j.elecom.2009.12.017

Wang, B., & Anzai, J. I. (2015). Recent progress in lectin-based biosensors. *Materials*, *8*(12), 8590–8607. https://doi.org/10.3390/ma8125478

Wang, L., Liu, Q., Hu, Z., Zhang, Y., Wu, C., Yang, M., & Wang, P. (2009). A novel electrochemical biosensor based on dynamic polymerase-extending hybridization for E. coli O157:H7 DNA detection. *Talanta*, *78*(3), 647–652. https://doi.org/10.1016/j.talanta.2008.12.001

Wang, Q., Zhou, Z., Zhai, Y., Zhang, L., Hong, W., Zhang, Z., & Dong, S. (2015). Label-free aptamer biosensor for thrombin detection based on functionalized graphene nanocomposites. *Talanta*, *141*, 247–252. https://doi.org/10.1016/j.talanta.2015.04.012

Wang, R., Ruan, C., Kanayeva, D., Lassiter, K., & Li, Y. (2008). TiO 2 nanowire bundle microelectrode based impedance immunosensor for rapid and sensitive detection of *Listeria monocytogenes*. *Nano Letters*, *8*(9), 2625–2631. https://doi.org/10.1021/nl080366q

Wang, Y., Deen, I., & Zhitomirsky, I. (2011). Electrophoretic deposition of polyacrylic acid and composite films containing nanotubes and oxide particles. *Journal of Colloid and Interface Science*, *362*(2), 367–374. https://doi.org/10.1016/j.jcis.2011.07.007

Wang, Y., Ye, Z., & Ying, Y. (2012). New trends in impedimetric biosensors for the detection of foodborne pathogenic bacteria. *Sensors*, *12*(3), 3449–3471. https://doi.org/10.3390/s120303449

Wang, Z., Zhang, X., Gu, J., Yang, H., Nie, J., & Ma, G. (2014). Electrodeposition of alginate/chitosan layer-by-layer composite coatings on titanium substrates. *Carbohydrate Polymers*, *103*(1), 38–45. https://doi.org/10.1016/j.carbpol.2013.12.007

Wiśniewska, M., Urban, T., Grządka, E., Zarko, V. I., & Gun'ko, V. M. (2014). Comparison of adsorption affinity of polyacrylic acid for surfaces of mixed silica-alumina. *Colloid and Polymer Science*, *292*(3), 699–705. https://doi.org/10.1007/s00396-013-3103-x

Yang, G. J., Huang, J. L., Meng, W. J., Shen, M., & Jiao, X. A. (2009). A reusable capacitive immunosensor for detection of *Salmonella* spp. based on grafted ethylene diamine and self-assembled gold nanoparticle monolayers. *Analytica Chimica Acta*, *647*(2), 159–166. https://doi.org/10.1016/j.aca.2009.06.008

Yang, L., & Li, Y. (2004). AFM and impedance spectroscopy characterization of the immobilization of antibodies on indium-tin oxide electrode through self-assembled monolayer of epoxysilane and their capture of *Escherichia coli* O157:H7. *Biosensors and Bioelectronics*, *20*(7), 1407–1416. https://doi.org/10.1016/j.bios.2004.06.024

Zhang, L., Huang, R., Liu, W., Liu, H., Zhou, X., & Xing, D. (2016). Rapid and visual detection of *Listeria monocytogenes* based on nanoparticle cluster catalyzed signal amplification. Biosensors and Bioelectronics, 86, 1-7. shttps://doi.org/10.1016/j.bios.2016.05.100

Zhang, Z., Zhang, S., He, L., Peng, D., Yan, F., Wang, M., & Fang, S. (2015). Feasible electrochemical biosensor based on plasma polymerization-assisted composite of polyacrylic acid and hollow TiO spheres for sensitively detecting lysozyme. *Biosensors and Bioelectronics*, *74*, 384–390. https://doi.org/10.1016/j.bios.2015.06.062

Zhong, H., Yuan, R., Chai, Y., Zhang, Y., Wang, C., & Jia, F. (2012). Non-enzymatic hydrogen peroxide amperometric sensor based on a glassy carbon electrode modified with an MWCNT/polyaniline composite film and platinum nanoparticles. *Microchimica Acta*, *176*(3–4), 389–395. https://doi.org/10.1007/s00604-011-0731-z